Geochimica et Cosmochimica Acta 343 (2023) 1–16

Contents lists available at ScienceDirect

Geochimica et Cosmochimica Acta

journal homepage: www.elsevier.com/locate/gca

# Marine sedimentary uranium to barium ratios as a potential quantitative proxy for Pleistocene bottom water oxygen concentrations

Kassandra M. Costa [a], Sune G. Nielsen [a,b], Yi Wang [a,b], Wanyi Lu [a], Sophia K.V. Hines [c], Allison W. Jacobel [d,e], Delia W. Oppo [a]

[a] Department of Geology and Geophysics, Woods Hole Oceanographic Institution, Woods Hole, MA, USA
[b] NIRVANA Laboratories, Woods Hole Oceanographic Institution, Woods Hole, MA, USA
[c] Department of Marine Chemistry and Geochemistry, Woods Hole Oceanographic Institution, Woods Hole, MA, USA
[d] Department of Earth and Climate Sciences, Middlebury College, Middlebury, VT, USA
[e] Department of Earth, Environmental and Planetary Sciences, Brown University, Providence, RI, USA

ARTICLE INFO

*Article history:*
Received 20 August 2022
Accepted 17 December 2022
Available online 21 December 2022
*Associate editor:* Natascha Riedinger

*Keywords:*
Bottom water oxygen
Sediment geochemistry
Uranium
Barium
Pelagic sediments
Pleistocene
Glacial-interglacial cycles

ABSTRACT

Oxygen is essential for marine ecosystems, and it is linked by respiration to carbon storage in the deep ocean. Reconstructing oxygen concentrations in the past has been limited by the absence of quantitative, rather than qualitative, proxies, but several new (semi-) quantitative oxygen proxies have recently been developed. In this study we explore the possibility of adding bulk sedimentary uranium (U) to this list by normalizing it to barium (Ba). First, U/Ba and bottom water oxygen concentrations are compared on a global scale, using a core top database, in pelagic environments greater than 200 m water depth. Then, the relationships between U/Ba and bottom water oxygen are examined on smaller spatial scales: within each ocean basin and regionally within the Eastern Equatorial Pacific, the Arabian Sea, and Western Equatorial Atlantic. At this regional scale, where secondary influences on the behavior of both U and Ba may be more spatially uniform, empirical piecewise linear calibrations are developed and subsequently tested on downcore records. U/Ba-based oxygen reconstructions generally agree with those derived from previously published alkenone preservation and benthic foraminiferal surface porosity records. Several limitations to the utility of U/Ba as a proxy for oxygen have also been identified. The proxy should only be applied in the uppermost sedimentary intervals that contain porewater sulfate to minimize barite diagenesis, and phosphorus contents should be monitored for the potential influence of apatite on uranium content. U/Ba is more successful at recording oxygen concentrations during mean glacial and interglacial periods than during climate transitions, when the timing and amplitude may be more sensitive to burndown and smoothing. Conservative errors on the calibrations result in the greatest utility of U/Ba in regions with relatively high oxygen concentrations (e.g., >50 μmol/kg) and large oxygen variability (±10 s of μmol/kg). Even with these caveats, U/Ba is only one of two quantitative oxygen proxies potentially capable of recording variability above 50 μmol/kg, and further investigation into its functionality in different environmental settings is worthwhile in the endeavor to reconstruct the full marine range of oxygen concentrations in the past.


## 1. Introduction

Oxygen concentrations are a primary chemical characteristic of the ocean, responsible not only for life in the deep but also for driving the biogeochemical cycles of C, N, P, Mn, Fe, and many other trace elements. As the oceans take up anthropogenic $CO_2$, oxygen concentrations are declining (Garcia et al., 1998; Stramma et al., 2008; Keeling et al., 2010) in part due to decreased solubility in warming waters (Garcia et al., 1998; Matear and Hirst, 2003), increased physical stratification (Palter and Trossman, 2018), and enhanced biological respiration (Oschlies et al., 2008). This complex, multivariate system is difficult to parameterize, and models generate disparate forecasts in terms of the sign, amplitude, and trend of oxygen concentrations in the Common Era and into the future (Stramma et al., 2012; Cabré et al., 2015; Fu et al., 2018). Constraining these parameters under past climate conditions is critical for developing the mechanistic understanding which will allow for more accurate predictions of how oxygen concentrations will change in the future.

*E-mail address:* kassandra.costa@whoi.edu (K.M. Costa)

https://doi.org/10.1016/j.gca.2022.12.022
0016-7037/

Recently, the development of new (semi-)quantitative oxygen paleo-proxies has refined our understanding of the temporal and spatial evolution of oxygen dynamics in the ocean over the glacial-interglacial cycles of the late Pleistocene (here defined as the last 500,000 years). These proxies include: 1) the carbon isotope gradient ($\Delta\delta^{13}C$) between epifaunal to shallow infaunal (*Cibicidoides* spp.) and deep infaunal (*Globobulimina* spp.) benthic foraminifera (McCorkle and Emerson, 1988; Hoogakker et al., 2015), 2) I/Ca in *Cibicidoides* spp. (Lu et al., 2020; Lu et al., 2021), 3) sedimentary alkenone preservation (Prahl et al., 1993; Rodrigo-Gámiz et al., 2016; Anderson et al., 2019; Jacobel et al., 2020), 4) surface porosity of *Cibicidoides* spp. (Rathburn et al., 2018; Lu et al., 2021; Lu et al., 2022), and 5) benthic foraminifera assemblages (Ohkushi et al., 2013; Tetard et al., 2017; Tetard et al., 2021; Sharon and Belanger, 2022). For example, during the last glacial maximum (LGM, 18,000–24,000 years ago, or 18–24 ka), it has been hypothesized that carbon sequestration in the deep ocean led to lower glacial oxygen concentrations in deep waters (Boyle, 1990; Sigman and Boyle, 2000; Sigman et al., 2010). Applications of the aforementioned five paleo-oxygen proxies in the deep Pacific and Atlantic not only support this hypothesis qualitatively, but the quantitative $\Delta\delta^{13}C$ and alkenone preservation proxies can also constrain the magnitude of oxygen loss to 65–100 μmol/kg. This change in oxygen can be translated to a change in deep ocean carbon storage of approximately 800 Pg carbon, using the stoichiometric relationship between the concentrations of oxygen and carbon via bacterial respiration (Anderson et al., 2019).

There are three main limitations to this new suite of quantitative proxies. First, none of the proxies explicitly distinguish between porewater oxygen concentrations and bottom water oxygen (BWO) concentrations. While oxygen concentration in porewaters are initially set by bottom waters, they may become decoupled if high organic carbon fluxes generate intense respiration in surficial sediments (<10 cm) that rapidly depletes oxygen concentrations in porewaters. As a result, when low oxygen concentrations are indicated by a proxy, that signal may reflect lower BWO concentrations (e.g., by reduced water mass ventilation or a change in water mass), lower porewater oxygen concentrations (e.g., by higher organic carbon delivery to the sediment), or a combination of the two. While the potential effects of organic carbon fluxes are often qualitatively monitored with independent proxies, this effect is not specifically incorporated into the proxy quantifications. Second, four out of five oxygen proxies ($\Delta\delta^{13}C$, I/Ca, surface porosity, and benthic assemblages) require the presence of specific foraminifera, namely *Cibicidoides* spp. While *Cibicidoides spp*. are generally abundant in the Atlantic (Jorissen et al., 2007), they can be scarce in, for example, regions with low export productivity (e.g., subtropical gyres, which comprise much of the Pacific Ocean). Furthermore, for $\Delta\delta^{13}C$, *Cibicidoides wuellerstorfi* and *Globobulimina affinis* do not always coexist in the same sedimentary layers, which can result in individually discontinuous and mutually incoincident $\delta^{13}C$ data. Finally, in regions (e.g., the deep Pacific or Southern Ocean) and times (e.g., interglacial periods, in the Pacific) when carbonate preservation is poor, the absence of foraminifera precludes the application of these proxies. The third major limitation is that four out of five proxies (alkenone preservation, I/Ca, surface porosity, and benthic assemblages) are sensitive to changes only at the lowest oxygen concentrations, generally <50 μmol/kg (e.g., Anderson et al., 2019; Lu et al., 2021, 2022). Therefore, large changes in oxygen concentrations that do not cross this threshold (e.g., from 250 μmol/kg to 150 μmol/kg) will not be recorded by these proxies. Currently only $\Delta\delta^{13}C$ can be applied to locations with oxygen concentrations consistently above 50 μmol/kg. However, at sites with both relatively high oxygen concentrations and low abundances of the requisite foraminifera, none of the five available quantitative oxygen proxies can be utilized.

In this study, we attempt, for the first time, to isolate the BWO signal in sedimentary uranium content by normalizing it to a proxy for organic carbon fluxes to the sediment. Uranium has previously been applied as a qualitative indicator of BWO variability in the past (Calvert and Pedersen, 1993; Sarkar et al., 1993; Frank et al., 2000; Jaccard et al., 2009; Martínez-Garcia et al., 2009), but converting uranium content to discrete BWO concentrations has been difficult due to its complex sedimentary geochemistry (see Section 2.1). Because bulk sedimentary uranium can be measured even when benthic foraminifera are rare or absent, its quantification could greatly expand the spatial and temporal domains for reconstructing BWO concentrations in the past. Using a core top compilation (Fig. 1), we examine the relationships between uranium, BWO, and organic carbon fluxes (parameterized using sedimentary barium content see Section 2.2). By normalizing uranium to barium (U/Ba), this proxy has advantages over previous approaches because 1) it accounts for dilution effects from variable sedimentation rates, 2) it is not dependent on lithogenic ratios, and 3) it identifies changes in uranium contents in excess of what is driven by organic carbon fluxes and so can be more confidently attributed to changes in (specifically) BWO concentrations. The data are evaluated at three spatial scales: global, ocean basin, and regional. Finally, we assess the proxy utility in three locations (the Eastern Equatorial Pacific, the Arabian Sea, and the Western Equatorial Atlantic) by applying the regionally-derived empirical relationships between U/Ba and BWO to downcore records and comparing the results with previously published independent oxygen reconstructions from $\Delta\delta^{13}C$ and benthic foraminifera surface porosity.

## 2. Background

### 2.1. Uranium systematics

Uranium is soluble in oxygenated seawater, and its long residence time (400,000 yrs) makes dissolved uranium concentrations quasi-conservative and scalable with salinity (Owens et al., 2011). Oxidized uranium (U[VI]) complexes with carbonate ions, predominantly in the uncharged form $Ca_2UO_2(CO_3)_3$ (Endrizzi and Rao, 2014). Within oxygenated porewaters, dissolved uranium maintains seawater concentrations, but as porewater oxygen concentrations are depleted by benthic respiration, soluble U(VI) reduces to insoluble U(IV) and precipitates as solid authigenic $UO_2$ (Anderson, 1982; Anderson et al., 1989; Morford and Emerson, 1999). Continued precipitation of uranium is supported by a diffusive flux from seawater, a practically unlimited reservoir in unrestricted marine systems, which can lead to substantial enrichments in uranium (1–10 μg/g, or ppm) relative to biogenic particles (for example, 3–4 μg/kg (or ppb) in foraminifera (Russell et al., 2004)). Thus, high uranium content has long been interpreted as a qualitative indicator of low oxygen concentrations in the sediments.

Ideally, authigenic uranium content (i.e., uranium precipitated in situ in excess of uranium from lithogenic particles) in surficial sediments could be directly converted to BWO concentrations, but the theoretical framework of uranium is complicated by other thermodynamic, kinetic, biological, and sedimentological processes. First, the baseline oxygen concentration at which uranium reduction occurs is poorly constrained, with some studies suggesting it co-occurs with iron reduction (Langmuir, 1978; Barnes and Cochran, 1990; Crusius et al., 1996; Zheng et al., 2002) while others suggest the lower redox potential required for sulfate reduction (Klinkhammer and Palmer, 1991). Furthermore, uranium reduction

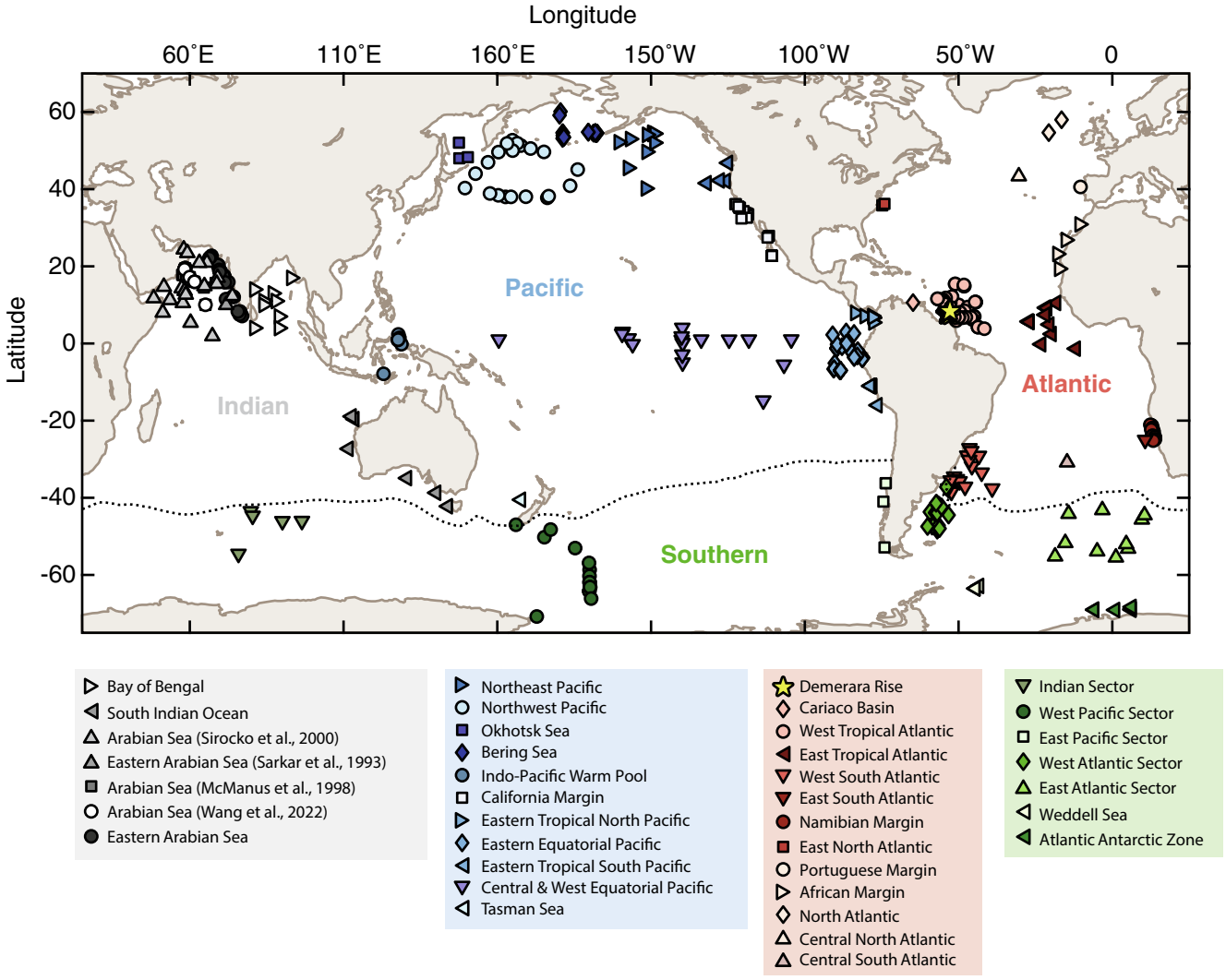


**Fig. 1. Map of coretop sediment locations**. Data are colorcoded by ocean basin: Indian (gray), Pacific (blue), Atlantic (red), and Southern (green). The northern boundary of the Southern Ocean (dashed line) is defined by the subtropical front (Orsi et al., 1995). New data from the Demerara Rise in the Western Equatorial Atlantic are shown as yellow stars. (For interpretation of the references to colour in this figure legend, the reader is referred to the web version of this article.)

may occur even when conditions are thermodynamically unfavorable. In laboratory experiments, adsorption onto mineral surfaces can facilitate abiotic uranium reduction (Kochenov et al., 1977; Nakashima et al., 1984; Liger et al., 1999), and dissimilatory iron-reducing and/or sulfate-reducing microorganisms (e.g., *Clostridium sp*., *Desulfovibrio sp*., *Shewanella* sp.) can catalyze uranium reduction as a byproduct of their chemolithotropic growth (Lovley et al., 1991; Lovley and Phillips, 1992; Francis et al., 1994; Ganesh et al., 1997; Sani et al., 2004, Lee et al., 2014). However, these experiments are usually conducted under "standard" conditions (e.g., 1 atm, 25 °C) that are not representative of conditions on the seafloor (e.g. 300–400 atm, 1–4 °C), and so their findings may or may not be directly applicable to the marine systems of interest in this study.

The complex chemistry of uranium in porewaters and sediments can be demonstrated by comparing theoretical profiles (e.g., Froelich et al., 1979) with observed profiles in an example pelagic core, EN433-2 (36.15°N, 74.06°W, 2648 m water depth, 270 μmol/kg bottom water oxygen) (Morford et al., 2009) (Fig. 2). Theoretically, porewater oxygen decreases with increasing depth in the sediment until oxygen concentrations reach zero. Anaerobic respiration may then consume Mn, resulting in increasing porewater concentrations of the soluble reduced species Mn(II) (Fig. 2A). Solid phase Mn oxides peak above the sediment horizon at which reduction commences (Fig. 2B). Rather than a sharp boundary, solid phase peaks tend to be broad as a result of bioturbation, which smooths sedimentary records over a depth range of, e.g., 6–10 cm in the pelagic ocean (Berger and Johnson, 1978; Cochran, 1985; Trauth, 2013). In contrast, the reduced species U(IV) is less soluble than the oxidized species U(VI), and porewater uranium decreases (Fig. 2A) and solid phase uranium increases (Fig. 2B) below the uranium reduction horizon.

The observed porewater and solid phase profiles in EN433-2 (Fig. 2C, D) demonstrate some similarities and some important differences from theoretical expectations. Where porewater oxygen concentrations reach zero (~4 cm), Mn reduction causes porewater Mn concentrations to start increasing with depth (Fig. 2C). Solid phase Mn peaks at ~3 cm, just above the sediment horizon where Mn reduction commences (Fig. 2D). Therefore, at this site, Mn behaves generally as expected from its theoretical predictions. However, uranium does not. Porewater uranium concentrations decrease monotonically from the sediment surface throughout the sediment profile (Fig. 2C), even when oxygen is still present, and this decrease starts shallower than the increase of Mn. Porewater uranium is still relatively high (~8 μmol/kg) when solid phase authigenic uranium content reaches its maximum

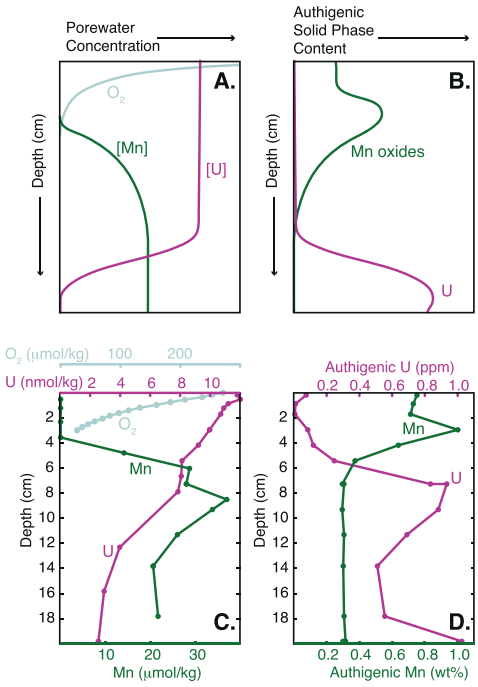


**Fig. 2. Theoretical vs observed profiles of trace metal concentrations in porewaters and authigenic phases.** Theoretical predictions for the relationship between oxygen, manganese, and uranium in porewaters (panel A) and authigenic solid phases (panel B), after (Froelich et al., 1979). Observed profiles (C, D) are shown for example pelagic core EN433-2 (36.15°N, 74.06°W, 2648 m water depth, 270 μmol/kg bottom water oxygen) (Morford et al., 2009). Authigenic uranium and manganese contents were calculated by subtracting from the total content a lithogenic component constrained with aluminum and average upper continental crust composition. (Taylor and McLennan, 1995). While observed Mn concentrations in both the porewaters and the authigenic phases (primarily Mn oxides) correspond fairly well with theoretical expectations, the uranium profiles diverge as a result of non-thermodynamic effects as discussed in Section 2.1.

(~0.9 ppm, 6–9 cm). This mismatch between theoretical and observed uranium behavior in sediments highlights the complications of using a purely thermodynamic redox model, which indeed has been described as "not appropriate for most sediments" (Burdige and Gieskes, 1983).

In addition, when considering sedimentary uranium across spatial gradients and/or over time, sedimentological properties like sedimentation rate, lithogenic flux and composition, and organic carbon fluxes can affect uranium content, complicating isolation of a purely BWO signal. For the same BWO concentration and organic carbon flux, sedimentary uranium contents may differ due to the dilution effects of variable sedimentation rates (i.e., high sedimentation rate sites would have lower uranium content than low sedimentation sites). On the other hand, at open ocean sites with low sedimentation, especially <2 cm/kyr, continuous exposure to relatively high oxygen bottom waters via bioturbation can cause authigenic uranium to reoxidize and diffuse out of the sediment (i.e., burndown), leaving behind no archival record of its precipitation at all (Mangini et al., 2001; Jacobel et al., 2017; Costa et al., 2018). The latter preservation bias is difficult to identify and even more challenging to account or correct for, and the primary solution is to avoid interpreting redox records from these low sedimentation sites (as demonstrated by Jacobel et al., 2020).

The dilution bias is generally amended by one of two approaches. First, linear mass accumulation rates integrate authigenic uranium content across a depth horizon to calculate the total authigenic uranium flux (aU flux) to the sediment. The main caveat to this approach is that it requires a well-constrained chronology and bulk sediment density, which may not be available. Alternatively, uranium content may be normalized to a lithogenic element (LE, such as aluminum or titanium), with the assumption that dilution will affect both elemental contents and thus cancel out. This ratio (U/LE) may be employed as such, or it can be converted to an enrichment factor (EF) by normalizing the observed U/LE ($U/LE_{obs}$) to the assumed U/LE of the lithogenic material ($U/LE_{lith}$) ($U_{EF} = U/LE_{obs} / U/LE_{lith}$). The main caveat to this approach is that it relies on constraining the lithogenic content and composition in order to isolate the fraction of uranium precipitated authigenically. The composition of the lithogenic component of marine sediments (i.e., $U/LE_{lith}$) varies on a regional scale as a function of the proximal crustal sources and transport pathways, but it is not always straightforward to pinpoint the specific $U/LE_{lith}$ at any one site. For this reason, it is likely that regional calibrations using uranium enrichment may work more successfully than global ones.

Finally, sedimentary uranium content, like all of the paleo-oxygen proxies, depends not just on BWO but also on the flux of reductants to the sediment, primarily in the form of organic carbon in the open ocean. Microbial respiration of organic matter lowers porewater oxygen concentrations relative to BWO concentrations, such that uranium may precipitate even though the overlying bottom waters are oxic. For example, uranium enrichment has been observed in the Eastern Equatorial Pacific (Singh et al., 2011), the California Margin (McManus et al., 1998), and the Bering Sea (Serno et al., 2014) at sites that all have BWO concentrations >90 μmol/kg. In some settings, particularly on continental margins, high organic carbon content (>2 wt% organic carbon, often >5 wt%) is the dominant control on porewater oxygen, and thus uranium precipitation is primarily interpreted as a productivity rather than oxygen signal (e.g., McManus et al., 2006). However, in the open ocean, sedimentary organic carbon content is much lower than on continental margins (e.g., Hayes et al., 2021; Lee et al., 2019), and so BWO can have a substantial influence on sedimentary uranium content.

In order to isolate the BWO signal, uranium content is normalized to a proxy for organic carbon fluxes to the sediment. While sedimentary organic carbon content may be the most intuitive normalization parameter, its relationship to export production from the photic zone is strongly overprinted by microbial respiration in the water column and sediments, such that in the open ocean generally <1 % of the organic carbon exported from the photic zone is actually preserved in the sediment record (Pilson, 2012). Preservation within the water column is driven by microbial respiration, the extent of which will depend on the type of organic matter (e.g., Lee et al., 2004), sinking rate (e.g., Armstrong et al., 2001), and mineral protection (e.g., Keil et al., 1994). Subsequently, in the sediment, organic carbon preservation depends primarily on oxygen concentrations as well as processes that affect exposure to oxygen like sedimentation rates and bioturbation (Canfield, 1994; Arndt et al., 2013). For example, high sedimentation rates quickly bury organic carbon, and, by limiting its exposure to high BWO concentrations, high organic carbon preservation in the sediment is possible (Müller and Suess, 1979; Hartnett et al., 1998). Since organic carbon preservation is itself dependent on oxygen concentrations, it would be circular to use organic carbon content to normalize uranium. Instead, we utilize barium as an independent proxy for organic carbon fluxes because, in the open ocean, its preservation is much less sensitive to oxygen concentrations (as discussed in the next section).

### 2.2. Barium systematics

In the open ocean, dissolved barium concentrations have nutrient-like spatial patterns akin to those of silica (Horner et al., 2015), with the highest concentrations (≤150 μmol/kg) in the deep Pacific (Carter et al., 2020; GEOTRACES Intermediate Data Product

Group, 2021). The solid phase of barium, barium sulfate (barite), is undersaturated in most of the ocean (Church and Wolgemuth, 1972; Monnin et al., 1999), and its precipitation in seawater should be thermodynamically unfavorable. Yet barite can be found throughout the water column throughout the global ocean (e.g., Bishop, 1988; Dehairs et al., 1980). Barite formation likely occurs in microenvironments within organic aggregates where facilitation by heterotrophic bacteria can locally overcome the impediment of undersaturation (Bishop, 1988; Bertram and Cowen, 1997; Ganeshram et al., 2003; Gonzalez-Muñoz et al., 2012; Horner et al., 2015; Martinez-Ruiz et al., 2019; Carter et al., 2020), potentially by increasing the barite saturation state as well as providing additional nucleation sites (Martinez-Ruiz et al., 2018). As the organic-rich particulates sink and disaggregate, barite may remineralize as a result of exposure to ambient under-saturated waters. The fraction of barite that is precipitated in the water column and survives to reach the seafloor ranges from 0 to 30 % as a function of both the organic matter flux and barite saturation state (Dymond et al., 1992; Paytan and Kastner, 1996).

Once barite reaches the seafloor, it may be susceptible to further remineralization as a result of redox processes within the sediment. Where oxygen concentrations are low and organic carbon fluxes are high, porewater sulfate can act as an oxidant for anaerobic respiration. Consequently, barite dissolves, the concentration of dissolved barium increases, and dissolved barium may diffuse upward in the sediment column (Von Breymann et al., 1992; Paytan and Kastner, 1996). If the depth of sulfate reduction is relatively shallow, then the dissolved barium in porewaters may diffuse upwards, potentially to the sediment–water interface, and the original deposition of barium as a function of export productivity may be distorted or lost entirely. Alternatively, if the sediment horizon where sulfate reduction occurs is relatively deep, then the dissolved barium may reprecipitate diagenetically upon reaching shallower, sulfate-replete porewaters (Torres et al., 1996), causing the barium enrichments to be shifted up-core. Redox-generated distortions in the barium sedimentary record can be diagnosed via morphological identification of diagenetic barite, evidence for anaerobic respiration, and/or the presence of sulfide species, such as pyrite ($FeS_2$). Constraining the depth in the sediment where preservation effects overprint the export productivity signal is important in determining the utility of barium as a normalization parameter for uranium.

The preservation of barium in the sediment is likely to vary from region to region and over time. In locations where organic carbon fluxes are high and/or BWO concentrations are low, sulfate reduction may occur at shallow depths in the sediment (e.g., <1 m). For example, in the Santa Barbara Basin, sulfate reduction commences within the top 5 cm of the sediments resulting in sulfate depletion in porewaters at 100–150 cm below the sediment–water interface (Kuwabara et al., 1999; Reimers et al., 1990; Reimers et al., 1996, Raven et al., 2016), and the coincident high sedimentation rates (~150 cm/kyr; Thorton, 1984) limit the viability of the barium proxy to at most a few hundred years (or not at all). On the other hand, porewater oxygen is present throughout the entire sediment column in regions like the South Pacific Gyre (D'Hondt et al., 2009; D'Hondt et al., 2015), and slow sedimentation rates (e.g., <1 cm/kyr) could potentially extend good barite preservation over timescales of millions of years (in which case the utility of U/Ba would instead be limited by the residence time of uranium). In the open ocean, BWO concentrations are typically high enough (e.g., >100 μmol/kg) and organic carbon fluxes are typically low enough (e.g., <1 wt%) that sulfate reduction is likely to be minimal in sediments that correspond to the late Pleistocene (Anderson et al., 2019; Singh et al., 2020). Despite this general observation, we strongly advise that, where possible, porewater sulfate concentrations be measured (or reconstructed) to ensure that barite preservation is maintained over the sediment depth range over which U/Ba is to be applied.

Assuming negligible diagenesis, sedimentary barite contents can be interpreted to reflect organic carbon fluxes. In practice, the mineral abundance of barite is often estimated by the excess barium content (exBa or $Ba_{xs}$), i.e. the total barium minus the barium fraction associated with lithogenic particles in the sediment. An empirical linear relationship has been proposed between barite (or excess barium) mass accumulation rates and organic carbon fluxes (Dymond et al., 1992; Francois et al., 1995; Paytan et al., 1996). The correlation is poor when a single function is assessed on a global scale (Schoepfer et al., 2015; Hayes et al., 2021), but the relationship is greatly improved when spatial variability in, for example, organic carbon to excess barium ratios ($C_{org}/Ba_{xs}$) and organic carbon remineralization rates are taken under consideration (see discussion in Carter et al., 2020). Stronger quantitative relationships between excess barium and organic carbon flux on the regional scale are another potential reason why the development of U/Ba as a quantitative proxy for BWO may work better in limited spatial settings. Consequently, in this study we primarily investigate U/Ba on the smaller spatial scales of individual ocean basins (Pacific, Atlantic, Indian, and Southern) and regions (Eastern Equatorial Pacific, Arabian Sea, and Western Equatorial Atlantic).

## 3. Methods

### 3.1. Compilation of previously published data

This study leverages several previously published databases. Core tops, analyzed by Wang et al. (2022), include the full spectrum of major and trace elements including U, Ba, and P. The core top Ba database of Hayes et al. (2021) was cross-referenced with the U-Th database of Costa et al. (2020) as well as the original publications in order to compile U, Ba, and P where available (Dorta and Rona, 1971; Sarin et al., 1979; Calvert and Price, 1983; Frank et al., 1995; McManus et al., 1998; Bonn et al., 1998; Ceccaroni et al., 1998; Weber, 1998; Veeh et al., 1999; Murray et al., 2000; Sirocko et al., 2000; Veeh et al., 2000; Pfeifer et al., 2001; Nameroff et al., 2002; Prakash Babu et al., 2002; Chase et al., 2003; Eagle et al., 2003; Neimann and Geibert, 2003; Anderson and Winckler, 2005; McManus et al., 2005; Gonneea and Paytan, 2006; Shigemitsu et al., 2007; Bradtmiller et al., 2007; Anderson et al., 2009; Mills et al., 2010; Singh et al., 2011; Anderson et al., 2014; Serno et al., 2014; Calvert et al., 2015; Costa et al., 2016; Hickey, 2016; Lippold et al., 2016; Loveley et al., 2017; Wang et al., 2022). Several additional sites were included for which both U and Ba were available. Unfortunately, all three elemental contents were not available at each site, with P being the most commonly missing element. As this study focuses on open ocean sediments, sites from the continental shelf (<200 m) were explicitly omitted. Modern BWO concentrations were extracted and averaged (mean) from three data products: World Ocean Atlas 2018 (Garcia et al., 2019), GLODAPv2 (Olsen et al., 2016), and WOCE (Gouretski and Koltermann, 2004), and thus they may differ slightly from the BWO concentrations used in the original publications.

### 3.2. New data from Demerara Rise

Sediment cores from the Demerara Rise, in the Western Equatorial Atlantic (7-9°N, 53-54°W, 383–3328 m water depth), were recovered in 2010 on the KNR197-3 cruise. BWO concentrations for these sites were extracted from data products as described above. Modern BWO concentrations are lowest at the shallowest depths (~120 μmol/kg at 400 m) and then increase monotonically

to ~260 μmol/kg by about 1750 m. Below 1750 m, BWO concentrations remain relatively constant at ~260 μmol/kg. Coretop samples from 14 sites comprise a total of 27 discrete measurements, in which two datapoints from the same site are true independent replicates sampled from different multicore barrels.

One downcore record covering the last 21 kyr was generated from KNR197-3-60GGC (8.4°N, 52.97°W, 2550 m). The chronology for this core is based on radiocarbon dating and benthic oxygen isotopes (Oppo et al., 2018).

Sediments were analyzed for uranium and barium content as well as isotopes of uranium and thorium (for $^{230}$Th constant flux normalization) via complete acid digestion. Samples (100 mg) and various reference materials (BIR-1, MESS-3, DTS-2B, SGR-1, NIST2702, MAG-1, SDO-1, NIST2711, BHVO- 2) were spiked with $^{229}$Th and $^{236}$U for isotopic analysis. Samples and reference materials were digested in perchloric, nitric, and hydrofluoric acids, and subsequently the solution was split 1:10 for bulk elemental and isotopic analyses. The isotopic aliquot was additionally processed with column chromatography (Fleisher and Anderson, 2003). Isotopes for both uranium and thorium were measured on an Element 2 ICP-MS at Lamont-Doherty Earth Observatory of Columbia University. Because most of these sites are too shallow to utilize thorium normalization (Costa et al., 2020), we do not discuss the thorium data further. Based on replicates of the internal sediment standard VIMS (Costa and McManus, 2017) average measurement precision was 3.3 % for U and 5.1 % for Ba.

The elemental aliquot was further diluted and then analyzed on a Thermo Scientific iCAP 7400 DUO at Brown University. Barium content was calibrated to the in-situ digested standard reference materials.

We do not perform a lithogenic correction in this study due to poorly constrained spatial variability in lithogenic source composition (Supplementary Text, Fig. S1). By including the lithogenic U and Ba, the U/Ba ratio will asymptotically approach a non-zero (implicit lithogenic) value at high oxygen concentrations where the authigenic uranium content may be negligible. At low oxygen concentrations, barium content would not go to zero even if all of the authigenic barite were remineralized. An advantage of this approach is that it limits the sensitivity of U/Ba to barite preservation at low oxygen conditions; i.e., uranium could be added infinitely, but barium removal would be finite. Therefore, total (uncorrected) U/Ba and oxygen could reasonably be made quantitative when applied to local and regional spatial scales.

Benthic foraminifera oxygen and carbon isotopes for *Globobulimina affinis* and *Cibicidoides* spp. were measured using a Finnegan MAT253 IRMS coupled to a Kiel Device at Woods Hole Oceanographic Institution. Typical analyses contained 1–5 specimens of *G. affinis* and 3–6 specimens of *Cibicidoides spp* from >212 μm coarse fraction. Species availability of *Cibicidoides spp*. in core tops was depth dependent, with *C. pachyderma* abundant at shallow sites (<1500 m) and *C. wuellerstorfi* abundant at deeper sites (Oppo et al., 2018). All data from the downcore site (KNR197-3-60GGC) are from *C. wuellerstorfi*. Data were converted to Vienna Pee Dee Belemnite using NBS-19 standards analyzed in each run. Average measurement precision (1σ), as determined by NBS-19 replicates, was ±0.05 ‰ for $\delta^{13}$C and ±0.08 ‰ for $\delta^{18}$O.

### 3.3. Statistical approach

Local calibrations for the Eastern Equatorial Pacific, Arabian Sea, and Western Equatorial Atlantic were created by regressing regional core top U/Ba onto modern BWO concentrations. An empirical relationship was defined using piecewise linear functions that allowed for up to four linear segments using a published MATLAB shape modeling script (D'Errico, 2022). The regression was run 1000 times, and for each iteration, the regression was based on a random selection of 90 % of the available U/Ba datapoints, in order to minimize the sensitivity of the results to any one datapoint. When more than one linear piece was utilized, the break point(s) between pieces were free-floating and determined objectively by the shape modeling script for each iteration. The trend lines are the mean and standard deviation of the 1000 iterations. After completing this process for 1 to 4 piece linear functions, the final trend line was selected as the one that minimized the root mean squared error (RMSE). An example of this process is demonstrated in Fig. S2.

In this study, the Holocene is defined as 0–6 ka, and the last glacial maximum is defined as 18–24 ka. All reported statistical significance values were determined by a two-tailed students *t*-test.

## 4. Results

### 4.1. New data from the Demerara Rise

New multicore top uranium contents range from 1.73 to 4.12 ppm and decrease monotonically with water depth ($p < 0.001$) (Fig. 3, Supplementary Data 1). Multicore top barium contents range from 337 to 508 ppm and have no statistically significant trend with depth ($p = 0.81$). Thus, decreasing U/Ba from the

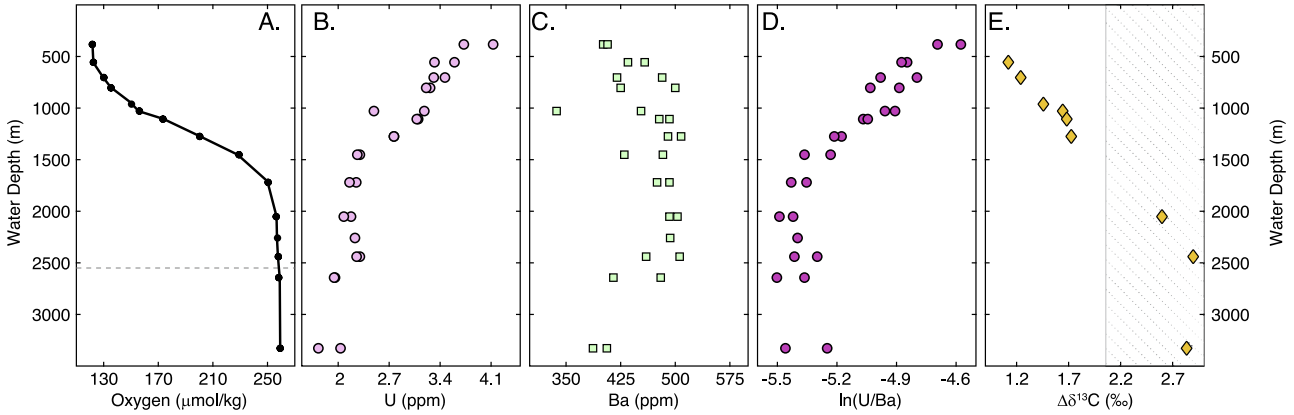


**Fig. 3. New multicore top U, Ba, and $\Delta\delta^{13}$C data from the Demerara Rise in the Western Equatorial Atlantic.** A) Modern bottom water oxygen concentrations, extracted from global data products as described in Section 3. Dashed gray line indicates the depth of the downcore records shown in Fig. 4. B) Total uranium content of core top samples. C) Total barium content of core top samples. D) The ratio of U/Ba shown in natural log space. E) $\Delta\delta^{13}$C in core top samples. Availability of the requisite foraminifera for this proxy limited the number of core tops for which data could be generated. Datapoints that fall within the gray hatched region exceed the upper limit of the $\Delta\delta^{13}$C calibration (Hoogakker et al., 2015).

shallowest multicore (383 m, ln(U/Ba) = −4.69 to −4.58) to the deepest multicore (3328 m, ln(U/Ba) = −5.46 to −5.25) is primarily driven by the uranium signal. A significant water depth trend is also present in $\Delta\delta^{13}C$, which increases from the shallowest multicore with data (556 m, $\Delta\delta^{13}C$ = −1.12) to the deepest multicore (3328 m, $\Delta\delta^{13}C$ = 2.83). The three $\Delta\delta^{13}C$ datapoints below 2000 m fall above the calibration range for $\Delta\delta^{13}C$ (Hoogakker et al., 2015).

New downcore uranium contents in KNR197-3-60GGC range from 2.25 to 5.42 ppm and decrease monotonically from the LGM to the core top (Fig. 4). The difference between the LGM mean value (5.17 ± 0.24 ppm) and the Holocene mean value (2.13 ± 0.2 3 ppm) is statistically significant ($p$ = 0.006). Downcore barium contents range from 311 to 564 ppm. The maximum barium content occurred at 9.3 ka, which was shortly followed by the minimum barium content at 6.6 ka. Glacial barium contents were fairly constant at 476–498 ppm, but barium content increased through the late Holocene from 322 ppm at 4.3 ka to 460–506 ppm in the multicore top. The variability in the late Holocene results in a statistically insignificant ($p$ = 0.30) difference between the LGM mean value and the Holocene mean value. Downcore U/Ba values were high during the last glacial maximum (ln(U/Ba) = −4.54 ± 0.03) (Fig. 4C). The values decreased through the deglaciation from 16.5 ka to ~10 ka. The resolution in this interval is too low to confidently affiliate deviations from a monotonic trend to particular millennial scale events. From ~10 ka to present, the U/Ba values were fairly constant with a late Holocene mean of ln(U/Ba) = −5.26 ± 0.10. The difference between the LGM mean value and the Holocene mean value is statistically significant ($p$ = 0.01).

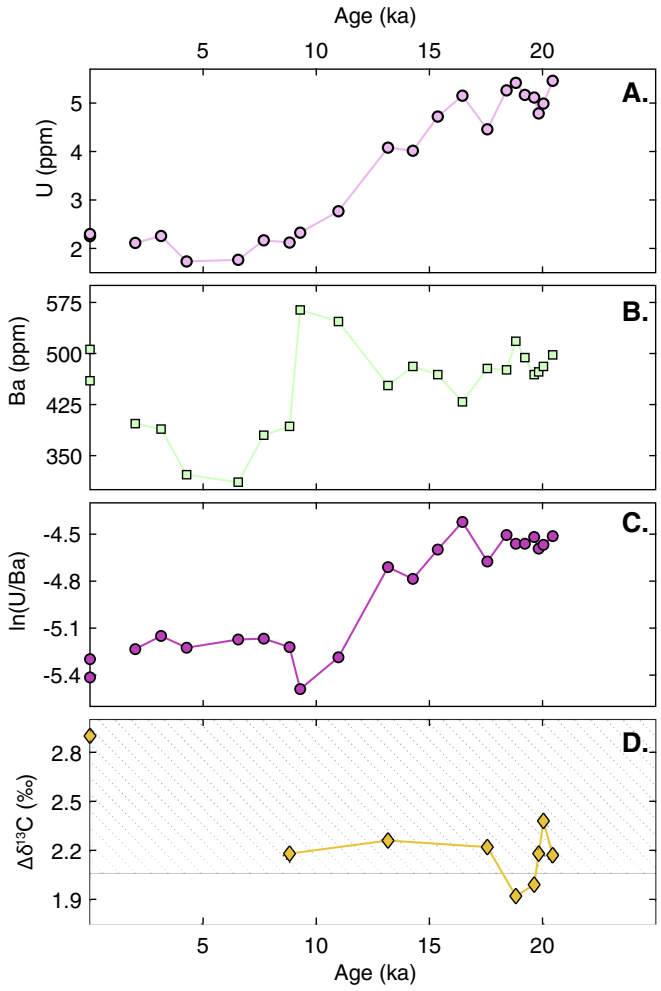


**Fig. 4. New downcore U, Ba, and $\Delta\delta^{13}C$ data from the Demerara Rise in the Western Equatorial Atlantic.** All data are from KNR197-3-60GGC (8.4°N, 52.97°W, 2550 m) except for the zero age datapoints, which are from the corresponding multicore KNR197-3-37MC. A) Total uranium content. B) Total barium content. C) The ratio of U/Ba shown in natural log space. D) $\Delta\delta^{13}C$ in the few downcore samples for which the requisite foraminifera for this proxy were available. The majority of the data exceed the upper limit of the $\Delta\delta^{13}C$ calibration (Hoogakker et al., 2015) (grey hatched region).

Downcore $\Delta\delta^{13}C$ data from KNR197-3-60GGC are at much lower resolution than U/Ba due to a paucity of coincident *G. affinis* and *C. wuellerstorfi* (Fig. 4D). Minimum $\Delta\delta^{13}C$ values of 2.12 ± 0.18 ‰ occurred during the LGM, and from 8.8 to 17.6 ka, $\Delta\delta^{13}C$ values were fairly constant at 2.22 ± 0.04 ‰. The absence of *G. affinis* precluded generating any late Holocene $\Delta\delta^{13}C$ values, but the corresponding multicore top $\Delta\delta^{13}C$ value is much higher (2.90 ‰) than any of the $\Delta\delta^{13}C$ values from the LGM and deglaciation. Nearly all $\Delta\delta^{13}C$ values exceed the calibration limit of the proxy.

### 4.2. Global data compilation

In the global coretop database, ln(U/Ba) ranges from −8.60 to −0.42 (mean −5.66), and BWO concentrations range from 0 to 269 μmol/kg (mean 147 μmol/kg) (Fig. 5). The relationship between U/Ba and BWO behaves as theoretically predicted, with a general trend towards higher U/Ba as BWO concentrations decrease, but the correlation between U/Ba and BWO on a global scale is poor ($R^2$ = 0.14, $p$ < 0.001). The highest U/Ba values (ln (U/Ba) > -3) occur in the Arabian Sea, the Namibian Margin, and the Indo-Pacific Warm Pool (IPWP). While the Arabian Sea is consistent with the general U/Ba to BWO relationship, the Namibian margin and Indo-Pacific Warm Pool are systematically anomalous, with U/Ba increasing at relatively constant BWO concentrations.

In the Arabian Sea, high U/Ba occurs at sites (513–611 m) that have notably high phosphorus contents (1.9–10.8 wt%, Supplementary Data 2). In this region, the high U/Ba values are driven primarily by high uranium content (17.7–63.4 ppm) relative to the rest of core top database (0.11–14 ppm, median 1.6 ppm) rather than low barium content. In the Arabian Sea, the high uranium and high phosphorus content have been linked to abundant fish debris (biogenic) and authigenic apatite (see Lu et al., 2022). Apatite (calcium phosphate) can contain high uranium content (e.g., 30–110 ppm; Baturin and Kochenov, 2001; Kochenov and Baturin, 2002), and if apatite is abundant in the sediment, it may inflate the bulk sedimentary uranium content above that which can be attributed to the authigenic precipitation of uranium based on BWO concentrations. Indeed, in the Arabian Sea, the uranium in apatite was found to contribute as much as 56 % of the total uranium in the sediment (Lu et al., 2022). We follow the methodology of Lu et al. (2022) to correct the Arabian Sea data for the uranium contributed by apatite, as a function of the phosphorus content in the sediment. The U/Ba of the high phosphorus samples (ln(U/Ba) = −2.20 to −0.49) decreased as a result of this correction (ln(U/Ba) = −2.76 to −1.31).

For samples that did not report phosphorus contents, the apatite correction could not be conducted, and instead ln(U/Ba) ≥ −2.20 was used as a cutoff to exclude samples with a high probability of having uranium contents that are inflated by apatite. This screening excluded 4 sites from the Arabian Sea.

On the Namibian Margin, there is a strong linear positive relationship between U/Ba and phosphorus ($R^2$ = 0.71, $p$ < 0.001) and no correlation with BWO ($R^2$ = 0.09, $p$ = 0.71). The high U/Ba values occur at shallow sites (216–710 m) that have high phosphorus contents (0.1–9.4 wt%, Supplementary Data 2). Here, barium contents are anomalously low (52–692 ppm, median 155 ppm) relative to the rest of core top database (70–7770 ppm, median 682 ppm) in addition to the sites having high uranium (5.0–360 ppm, median

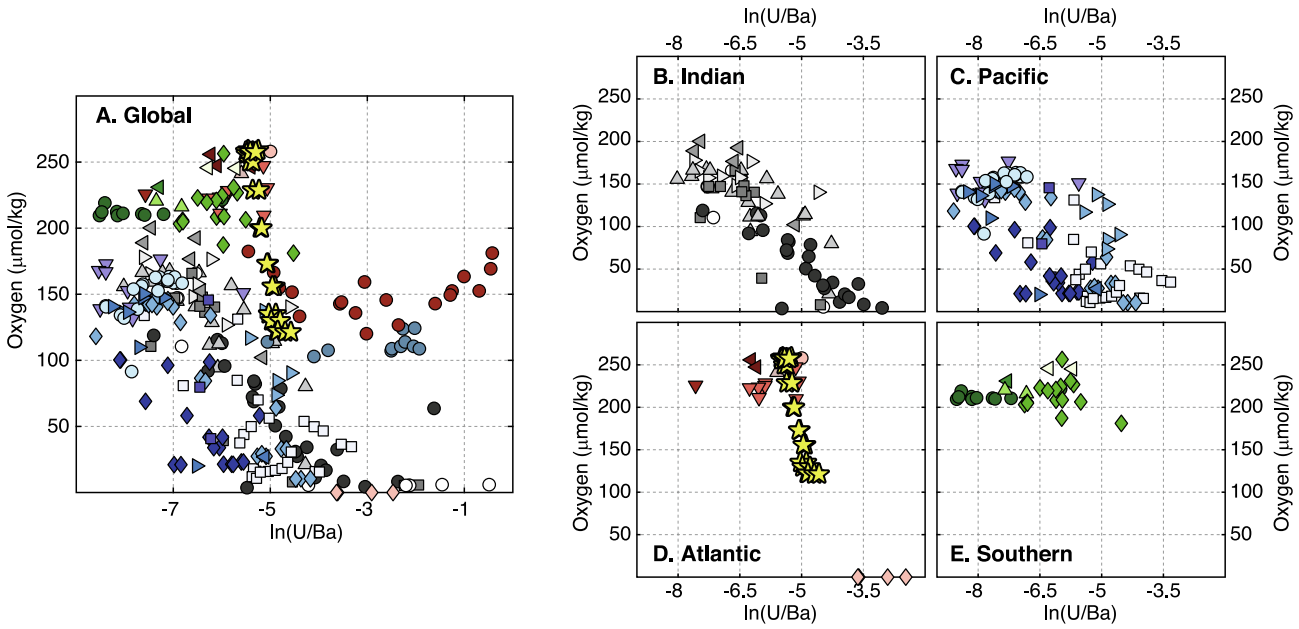


**Fig. 5. Relationship between U/Ba and oxygen on global and ocean basin scale.** Symbols are as in Fig. 1. New data from the Demerara Rise are shown as yellow stars. Note that x-axes are natural log while y-axes are linear. U/Ba generally increases as oxygen concentrations decrease. Two regions systematically fall off this trend: the Namibian Margin (maroon circles) and the Indo-Pacific Warm Pool (blue circles), where relatively high ln(U/Ba) values correspond to oxygen concentrations between 100 and 200 μmol/kg. Panels B-E show ocean basin scale relationships between U/Ba and oxygen (see text for details). The Namibian Margin and Indo-Pacific Warm Pool have been excluded from the Atlantic and Pacific, respectively. (For interpretation of the references to colour in this figure legend, the reader is referred to the web version of this article.)

19 ppm). Unlike the Arabian Sea, sedimentary phosphorus in this region is predominantly found as organic phosphorous rather than in apatite (Küster-Heins et al., 2010), and this phosphorus phase is not associated with particularly high uranium content (Kochenov and Baturin, 2002). The high U/Ba values may be a function of sulfate reduction leading to barite undersaturation and depressing barium content below what would be expected for this highly productive upwelling region (Brüchert et al., 2003). As a result, the U/Ba proxy is not effective as a BWO proxy, and we exclude these data and do not discuss them further.

In the IPWP, elevated U/Ba values show no correlation with BWO ($R^2$ = 0.31, $p$ = 0.35) or phosphorus ($R^2$ = 0.40, $p$ = 0.23). Uranium contents (3.3–8.7 ppm) are slightly elevated above the rest of the database, but it is the exceptionally low barium contents (39–66 ppm, median 42 ppm) that are primarily causing the high U/Ba values. As in the Namibian margin, the IPWP likely experiences sulfate reduction that negates the utility of barium as an export productivity proxy (Middelburg, 1991). As a result, U/Ba is not effective as a BWO proxy in this region, and we exclude these data and do not discuss them further.

Adjusting for apatite-bound uranium and excluding the sites as described above, the global correlation (log-linear) slightly improves for sedimentary U/Ba and BWO concentrations ($R^2$ = 0.25, $p$ < 0.001). The relationship between U/Ba and BWO improves substantially when the data are separated into different ocean basins (Fig. 5B-E). U/Ba and BWO are strongly correlated (log-linear) in the Indian Ocean (n = 80, $R^2$ = 0.73, $p$ < 0.001), the Pacific Ocean (n = 119, $R^2$ = 0.56, $p$ < 0.001), and the Atlantic Ocean (n = 46, $R^2$ = 0.63, $p$ < 0.001). For the Southern Ocean, the sites included in this study only cover a narrow range of BWO concentrations, and thus the correlation between U/Ba and BWO is predictably negligible (n = 32, $R^2$ = 0.01, $p$ = 0.63).

## 5. Discussion

Qualitatively, U/Ba increases as a function of BWO concentrations, but the spread of the data (particularly below ln(U/Ba) = −5) precludes the quantitative use of the proxy on a global scale. This limitation is not unexpected given the numerous regionally specific effects on both uranium and barium, as discussed in Section 2. Zooming in on smaller spatial scales should provide more robust and reasonably quantifiable relationships between U/Ba and BWO concentrations as the regional factors become more uniform and/or better constrained. In the next section, we explore the potential efficacy of U/Ba calibrations in three regions (Eastern Equatorial Pacific, Arabian Sea, and Western Equatorial Atlantic) where independent BWO reconstructions from other proxies are available for intercomparison.

### 5.1. Test cases for regional U/Ba quantification of oxygen concentrations

#### 5.1.1. Eastern Equatorial Pacific

First, we investigate U/Ba in the Eastern Equatorial Pacific (EEP) using data from ODP Leg 202 Site 1240 (0.02 °N, −86.5°E, 2921 m; Fig. 6A, yellow star), where Jacobel et al. (2020) quantitatively reconstructed BWO concentrations over the past 150,000 years using $\Delta\delta^{13}C$ (Fig. 6C). This timespan corresponds to the upper ~17 m of the sediment column at this site, over which porewater sulfate concentrations are relatively stable (Shipboard Scientific Party, 2003) and suggest minimal impact of sulfate reduction on barite preservation.

Past BWO concentrations were found to be significantly lower ($p$ < 0.01) in glacial periods than in interglacial periods (Fig. 6E, F). For example, the LGM (115 ± 2.9 μmol/kg) had about 100 μmol/kg lower BWO concentrations than in the Holocene (215 ± 9.8 μmol/kg). Low glacial BWO concentrations were qualitatively corroborated with high alkenone contents (Calvo et al., 2011) and high authigenic uranium contents (Jacobel et al., 2020) that were independent from variability in export productivity. However, quantitative discrepancies between Holocene (215 ± 9.8 μmol/kg) and modern (121 ± 4.7 μmol/kg) BWO concentrations and between glacial $\Delta\delta^{13}C$-based (115 ± 2.9 μmol/kg) and glacial alkenone-based (<50 μmol/kg) BWO concentrations suggest that

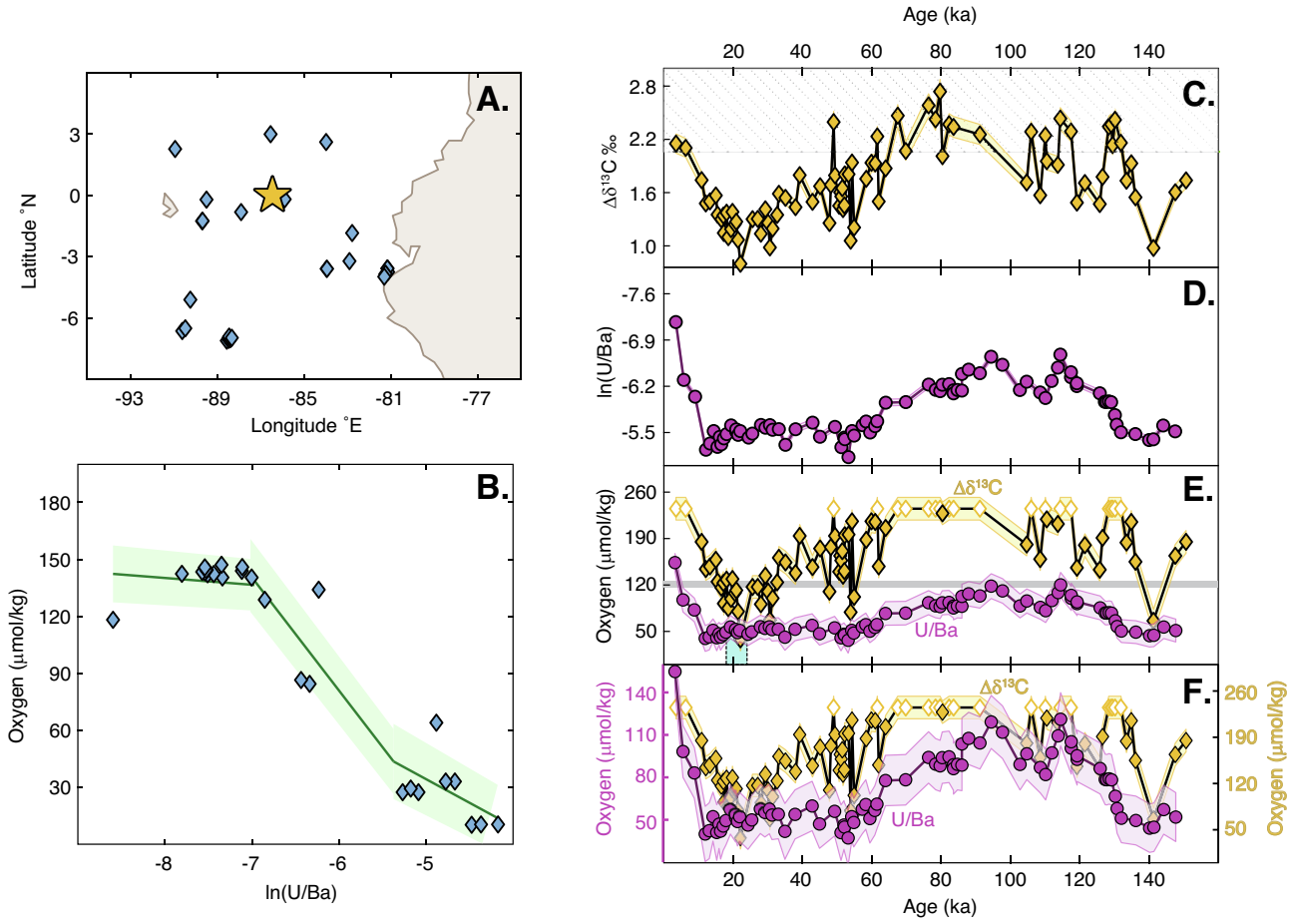


**Fig. 6. Eastern Equatorial Pacific calibration test data.** (A) Map showing the coretop sites used in the regional calibration (Loveley et al., 2017; Wang et al., 2022; Weber, 1998). Yellow star is the location of the downcore record from ODP Site 1240 (0.02 °N, −86.5°E, 2921 m). (B) The calibration is comprised of three linear functions (Table 1). (C) Raw $\Delta\delta^{13}C$ data from ODP Site 1240. Datapoints that fall within the gray hatched region exceed the limits of the $\Delta\delta^{13}C$ calibration (Hoogakker et al., 2015). (D) Raw U/Ba data from ODP Site 1240. All datapoints fall within the range of the calibration shown in panel B. (E) Calibrated $\Delta\delta^{13}C$ (yellow diamonds) and U/Ba (pink circles). Shaded regions show 1σ error. Data that fell outside the calibration for $\Delta\delta^{13}C$ were set to the maximum calibration limit (open diamonds). Gray line shows the modern bottom water oxygen concentration at ODP Site 1240. Blue box indicates the alkenone-based glacial oxygen concentrations of <50 µmol/kg proposed by Anderson et al. (2019). (F) Same as panel E, except that the two proxies are shown on independent y-axes to highlight the similar trends despite different absolute values. All downcore records have been previously published by Jacobel et al. (2020). (For interpretation of the references to colour in this figure legend, the reader is referred to the web version of this article.)

the $\Delta\delta^{13}C$ proxy may be susceptible to a positive bias (i.e., BWO concentrations that are too high). This effect may arise as a result of anaerobic processes that contribute additional negative $\delta^{13}C$ to *G. affinis* (McCorkle and Emerson, 1988; Piña-Ochoa et al., 2010; Nomaki et al., 2015; Jacobel et al., 2020), such as functional or facultative denitrification conducted by *G. affinis* itself. Holding *C. wuellerstorfi* $\delta^{13}C$ constant, a more negative *G. affinis* $\delta^{13}C$ generates a more positive $\Delta\delta^{13}C$ that in turn yields BWO concentrations that are too high. Empirically, better alignment with modern BWO concentrations and with glacial alkenone-based BWO reconstructions at ODP Site 1240 could be obtained by shifting the $\Delta\delta^{13}C$-based oxygen concentrations lower by 65–100 µmol/kg (greater offset in interglacial periods). This inter-proxy inconsistency motivates developing another quantitative proxy capable of recording variability in BWO concentrations above 50 µmol/kg.

To test the viability of U/Ba as a quantitative BWO proxy in this region, we subsampled the Pacific dataset (Fig. 5C) for only those core tops within the EEP (Fig. 6A). The regional calibration was generated as described in the methods (also see Fig. S2) and is comprised of three linear functions (Table 1) covering a BWO range from 16 to 142 µmol/kg (ln(U/Ba) = −4.17 to −8.60) (Fig. 6B). The greatest sensitivity (highest slope) occurs between 52 and 136 µmol/kg, although this range is constrained by only a few datapoints. We then applied this calibration to the previously published uranium and barium data of Jacobel et al. (2020) (Fig. 6D). The variability in downcore ln(U/Ba) record at this site spans a wide range (−5.24 to −7.17, Fig. 6D), but all the data fall within the range of the calibration. BWO concentrations comparable to modern values (121 ± 4.7 µmol/kg) occurred in interglacial periods like the Holocene (126 ± 11 µmol/kg) and MIS 5 (110–120 ka, 100 ± 6 µmol/kg) (Fig. 6E, F). BWO concentrations were significantly lower ($p$ < 0.01) in glacial periods like the LGM (52 ± 7 µmol/kg) and MIS 6 (135–145 ka, 49 ± 9 µmol/kg).

The overall patterns of BWO variability reconstructed from U/Ba and $\Delta\delta^{13}C$ are remarkably similar over the past two glacial-interglacial cycles. Both proxies indicate that BWO concentrations were lower in glacial periods than in interglacial periods, by 100 ± 10 µmol/kg from $\Delta\delta^{13}C$ and 64 ± 8 µmol/kg from U/Ba. Absolute BWO concentrations derived from U/Ba are almost always lower than those from $\Delta\delta^{13}C$, but they align better with both modern BWO concentrations and with the glacial alkenone-based BWO concentrations (<50 µmol/kg). Considering the aforementioned hypothesis of Jacobel et al. (2020) that the $\Delta\delta^{13}C$-based BWO concentrations may be biased too high, it is possible that, in this region, U/Ba provides more accurate quantification of BWO concentrations in the past.

**Table 1**
Regional calibration functions of the form BWO = m ± Δm * ln(U/Ba) + b ± Δb.

| **Eastern Equatorial Pacific** | | | | | |
|---|---|---|---|---|---|
| **Piece #** | **Applicable ln(U/Ba) range** | **m** | **Δm** | **b** | **Δb** |
| 1 | −8.60 to −7.06 | −3.59 | 1.29 | 111.4 | 10.0 |
| 2 | −7.06 to −5.46 | −59.5 | 1.94 | −276.4 | 12.2 |
| 3 | −5.46 to −4.17 | −24.9 | 2.72 | −90.5 | 13.1 |
| **Arabian Sea** | | | | | |
| **Piece #** | **Applicable ln(U/Ba) range** | **m** | **Δm** | **b** | **Δb** |
| 1 | −7.67 to −6.26 | −11.6 | 0.99 | −58.0 | 6.93 |
| 2 | −6.26 to −4.87 | −76.1 | 1.04 | −343.3 | 5.87 |
| 3 | −4.87 to −1.31 | −8.50 | 2.26 | −9.27 | 10.4 |
| **Western Equatorial Atlantic** | | | | | |
| **Piece #** | **Applicable ln(U/Ba) range** | **m** | **Δm** | **b** | **Δb** |
| 1 | −5.50 to −4.12 | −194.6 | 1.25 | −800.5 | 6.06 |
| 2 | −4.12 to −2.47 | −1.63 | 1.04 | 4.02 | 3.53 |

On the other hand, $\Delta\delta^{13}C$ likely has the advantage over uranium-based proxies for accurately recording the timing of transitions between different BWO mean states. At ODP1240, $\Delta\delta^{13}C$ indicates that relatively high BWO concentrations persisted from 125 to 60 ka, then decreased to a minimum at ~22 ka, and subsequently increased into the Holocene. U/Ba suggests that interglacial BWO concentrations started to decline at 94 ka, then maintained low glacial concentrations from 60 to 12 ka, and subsequently rose abruptly into the Holocene. This discrepancy in timing is likely driven by diagenetic remobilization of uranium (i.e. burndown, see Section 2.1). At this site, the premature decline of U/Ba out of the last interglacial period may be attributed to dissolution and downcore reprecipitation of high glacial uranium contents, as demonstrated by Jacobel et al. (2020) in the Equatorial Pacific. Consequently, the application of U/Ba may only be appropriate for capturing the amplitude of BWO variability between mean states (e.g., the LGM vs the Holocene) rather than constraining the timing or amplitude of transitions.

We propose that the most robust reconstructions of BWO in the EEP can be obtained by the combination of $\Delta\delta^{13}C$ and U/Ba. The BWO concentrations derived from $\Delta\delta^{13}C$ capture the timing of transitions, while U/Ba may provide better constraints on the absolute BWO concentrations. Furthermore, substantial discrepancies between the two proxies can identify regions and time periods where $\Delta\delta^{13}C$ may be affected by anaerobic processes like sulfate reduction or denitrification (by *G. affinis* or other denitrifiers). For example, at ODP1240, the inter-proxy offset appears larger in interglacial periods ($\Delta\delta^{13}C$-based BWO concentrations are higher than U/Ba-based BWO by ~100 μmol/kg) than in glacial periods (higher by ~60 μmol/kg). While it may be expected that anaerobic respiration would be greater in glacial periods when absolute BWO concentrations were lower, this effect may instead be more sensitive to organic carbon fluxes, which were higher in interglacial periods than in glacial periods (Jacobel et al., 2020). There is certainly more work to be done to better understand the intra-proxy mechanics and inter-proxy differences; both proxies would benefit from larger and more robust calibration datasets. Yet, empirically, the utility of U/Ba as a quantitative proxy for BWO appears promising in the EEP.

### 5.1.2. Arabian Sea

A multiproxy (benthic foraminiferal surface porosity, $\Delta\delta^{13}C$, benthic I/Ca, aU) reconstruction of BWO was generated by Lu et al. (2022) for the last 30,000 years at site TN41-8PG/JPC (17.8°N, 57.5°E, 761 m) (Fig. 7). This timespan corresponds to the upper ~130 cm of the sediment column at this site. At nearby ODP Leg 117 Site 727 (17.8°N, 57.6°E, 915 m), porewater sulfate concentrations decrease from 25 mmol/L (at 600 cm sediment depth) to 1.6 mmol/L (at 3590 cm sediment depth) (Shipboard Scientific Party, 1979), but no data are provided shallower than 600 cm. Another nearby site, boxcore NIOP484 (19.5°N, 58.43°W, 527 m), shows relatively constant porewater sulfate concentrations over the ~30 cm length of the core (Schenau et al., 2001), and subsequent studies on the barium content of the accompanying piston core found no evidence for porewater sulfate depletion or barium diagenesis in sediments covering the past 30,000 years (~500 cm) (Reichart et al., 2002). Therefore, it seems reasonable to assume that barite preservation at TN41-8PG/JPC is not affected either.

Lu et al. (2022) determined that benthic foraminiferal surface porosity was the most robust paleo-BWO proxy in this region, and porosity-based BWO concentrations were found to be significantly higher ($p$ = 0.03) in the LGM (20 ± 7.7 μmol/kg) than in the Holocene (7 ± 4.7 μmol/kg). $\Delta\delta^{13}C$ also captured a decline in BWO from the LGM to the Holocene, but it suggested unrealistically high BWO concentrations (LGM 91 ± 14 μmol/kg; Holocene 51 ± 23 μmol/kg) that could be attributed to the positive bias on $\Delta\delta^{13}C$, as observed in the EEP (Section 5.1.1). The semi-quantitative benthic I/Ca and sedimentary aU corroborated that BWO concentrations at this site have remained under the proposed threshold of 50 μmol/kg over the past 30,000 years, but neither proxy was able to detect BWO variability below those limits (Lu et al., 2022). Overall, low BWO concentrations (<30 μmol/kg) that may have decreased since the LGM would be consistent with (generally qualitative) evidence for more ventilated oxygen minimum zones in the LGM relative to the Holocene in the Arabian Sea (Altabet et al., 2002; Gaye et al., 2018) and globally (e.g., Erdem et al., 2020; Jaccard and Galbraith, 2012; Tetard et al., 2017).

To test the viability of U/Ba as a quantitative BWO proxy in this region, we subsampled the Indian Ocean dataset (Fig. 5A) for only those core tops within the Arabian Sea (Fig. 7A). The regional calibration was generated as described in the methods, with a three-piece linear function (Table 1) providing the minimum RMSE. The calibration covers a BWO range from 2.9 to 149 μmol/kg (ln(U/Ba) = −1.31 to −7.67) and has the greatest sensitivity between 32 and 122 μmol/kg (Fig. 7B). The variability in the downcore ln(U/Ba) record at this site is small (−3.87 to −2.77, Fig. 7D) and, unfortunately, within the lowest sensitivity part of the calibration. The result is constant BWO concentrations of around 19 μmol/kg over the past 30,000 years (Fig. 7E). Due to the relatively large error (~13 μmol/kg), there is no significant difference at any time between U/Ba-based and modern BWO concentrations (Holocene $p$ = 0.19; LGM $p$ = 0.16) or between U/Ba-based and porosity-based BWO concentrations (Holocene $p$ = 0.08; LGM $p$ = 0.95). Unsurprisingly, the U/Ba proxy could not register a significant ($p$ = 0.58) difference between the LGM (21 ± 7.6 μmol/kg) and the Holocene (18 ± 6.4 μmol/kg).

Like in the EEP, U/Ba seems to more reliably capture absolute BWO concentrations than relative temporal trends. BWO

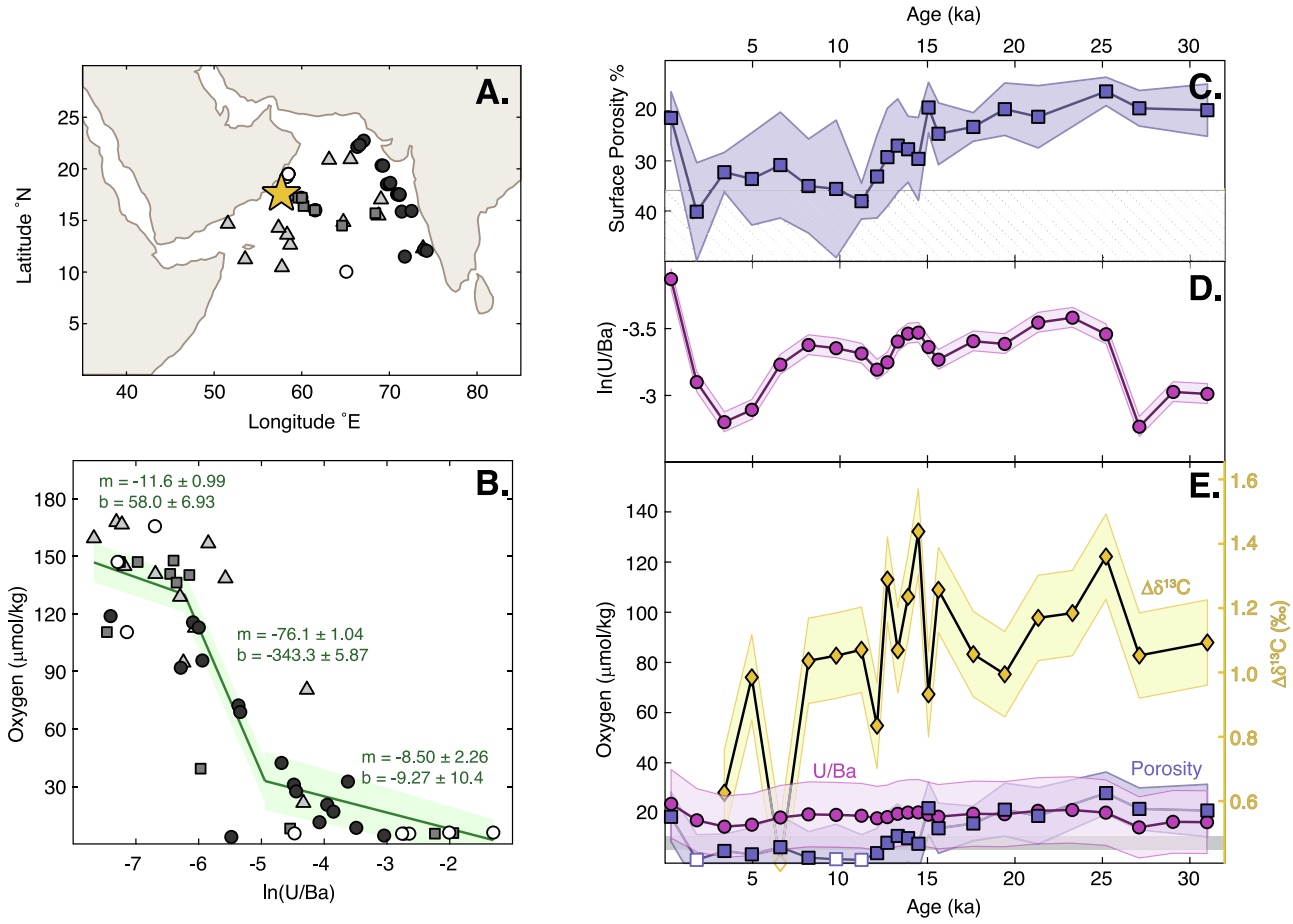


**Fig. 7. Arabian Sea calibration test data.** (A) Map showing the coretop sites used in the regional calibration (Lu et al., 2022; McManus et al., 1998; Prakash Babu et al., 2002; Sirocko et al., 2000). Yellow star is the location of the downcore record from TN41-8PG/JPC (17.8°N, 57.5°E, 761 m). (B) The calibration is comprised of three linear functions (Table 1). (C) Raw surface porosity record from TN41-8PG/JPC. Datapoints that fall within the gray hatched region exceed the limits of the surface porosity calibration (Lu et al., 2022). (D) Raw U/Ba data from TN41-8PG/JPC. (E) Calibrated surface porosity (blue squares) and U/Ba (pink circles). Yellow diamonds show $\Delta\delta^{13}C$ for comparison, in which the right yellow y-axis provides the raw (uncalibrated) values and the left black y-axis provides the calibrated oxygen concentrations. Shaded regions show 1σ error. Data that fell outside the calibration for $\Delta\delta^{13}C$ were set to the maximum calibration limit (open symbols). Gray line shows the modern bottom water oxygen concentration at TN41-8PG/JPC. All downcore records are from Lu et al. (2022). (For interpretation of the references to colour in this figure legend, the reader is referred to the web version of this article.)

concentrations persistently below 30 µmol/kg at this site match the conclusions of Lu et al. (2022) based on aU. They interpreted aU as a semiquantitative BWO proxy such that at their core site aU content >3 ppm reflected BWO concentrations below 30 µmol/kg. This threshold behavior is consistent with the slope change to lower sensitivity at 30 µmol/kg in the regional Arabian Sea U/Ba calibration, and it strongly suggests that U/Ba is not an effective quantitative proxy in regions where BWO concentrations have likely remained below 30 µmol/kg in the past, such as in oxygen minimum zones. Considering that there are existing quantitative (e.g., porosity, benthic foraminifera assemblages) and semiquantitative (e.g., benthic I/Ca) proxies that are more suitable for these low BWO concentrations, we propose that future proxy development of U/Ba focuses primarily on regions, like the EEP, with high BWO concentrations (e.g., >50 µmol/kg) and large BWO variability (±10 s of µmol/kg).

### 5.1.3. Western Equatorial Atlantic

Finally, we test new $\Delta\delta^{13}C$ and U/Ba from the deep Western Equatorial Atlantic (WEA) at site KNR197-3-60GGC (8.4°N, 52.97°W, 2550 m) over the last 20,000 years. This timespan corresponds to the upper ~50 cm of the sediment column at this site. Nearby core GeoB4418-3 (9.26°N, 54.06°W, 2495 m) has nearly constant sulfate concentrations over the upper ~7 m at 27.2 ± 0.8 mmol/kg (Kasten, 2004), and so we expect that the barite content at our site is well-preserved in the sediment.

Modern BWO concentrations are 260 µmol/kg, which is above the calibration limit of $\Delta\delta^{13}C$ (235 µmol/kg, $\Delta\delta^{13}C$ = 2.02 ‰; Hoogakker et al., 2015). Indeed, seven out of nine $\Delta\delta^{13}C$ datapoints fall outside the calibration range (Figs. 4D and 8). The two datapoints within the calibration range may indicate that BWO concentrations were lower (200 ± 12 µmol/kg) than modern during the last glacial maximum (18.8–19.6 ka), but just 1 kyr earlier (19.6–20.5 ka) BWO concentrations were still higher than 235 µmol/kg. Because the majority of the $\Delta\delta^{13}C$ values are outside of the calibration, this proxy is ineffective for reconstructing BWO concentrations. Without $\Delta\delta^{13}C$, there are no previously established proxies that are capable of operating at the high BWO concentrations in this region.

U/Ba could potentially address this issue. To test the viability of U/Ba as a quantitative BWO proxy in this region, we subsampled the Atlantic Ocean dataset (Fig. 5D) for only those core tops within the WEA (Fig. 8A). The regional calibration was generated as described in the methods, and it is comprised of two linear functions (Table 1, Fig. 8B) covering a BWO range from 0 to 273 µmol/kg (ln(U/Ba) = −2.47 to −5.50. The segment covering

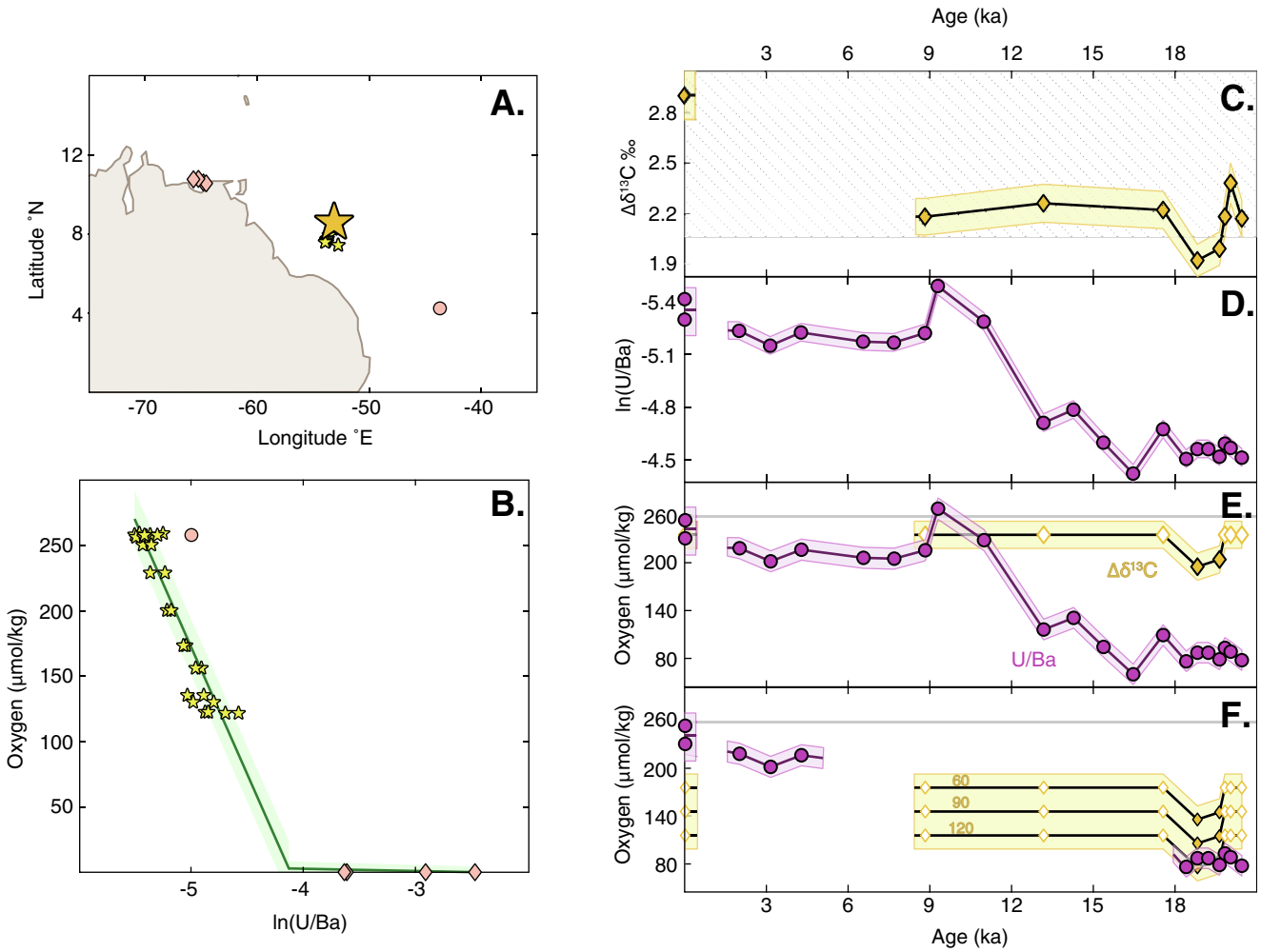


**Fig. 8. Western Equatorial Atlantic calibration test data**. (A) Map showing the coretop sites used in the regional calibration. Small yellow stars are new multicore data from this study, and the large yellow star is the location of the downcore record from KNR197-3-60GGC (8.4°N, 52.97°W, 2550 m). Pink circle is GeoB1515 (Pfeifer et al., 2001). Pink diamonds are from the Cariaco Basin (Calvert et al., 2015; Dorta and Rona, 1971). (B) The calibration is comprised of two linear functions (Table 1). (C) Raw $\delta^{13}C$ data from KNR197-3-60GGC. Datapoints that fall within the gray hatched region exceed the limits of the $\Delta\delta^{13}C$ calibration (Hoogakker et al., 2015). The zero age datapoint is from the corresponding multicore KNR197-3-37MC. (D) Raw U/Ba data from KNR197-3-60GGC. (E) Calibrated $\Delta\delta^{13}C$ (yellow diamonds) and U/Ba (pink circles). Shaded regions show 1σ error. Data that fell outside the calibration for $\Delta\delta^{13}C$ were set to the maximum calibration limit (open diamonds). Gray line shows the modern bottom water oxygen concentration at KNR197-3-60GGC. (F) Hypothetical $\Delta\delta^{13}C$-based oxygen reconstructions if the record were adjusted downwards by 60, 90, or 120 µmol/kg. U/Ba-based oxygen reconstructions (as in panel E) are only shown for the LGM (18–21 ka) and late Holocene (0–6 ka). (For interpretation of the references to colour in this figure legend, the reader is referred to the web version of this article.)

the lowest BWO concentrations is defined by sites at sulfidic depths (i.e., BWO = 0) in the Cariaco Basin, and so they should be evaluated with caution. The greatest sensitivity occurs in the most constrained segment from 137 to 273 µmol/kg (ln(U/Ba) = −4.85 to −5.5), which is where most of the downcore ln(U/Ba) values lie (−4.42 to −5.49, Fig. 8D). While the mean late Holocene value (224 ± 6 µmol/kg) is significantly lower ($p < 0.01$) than the modern BWO concentrations, the multicore top reconstructed BWO concentration (253 ± 13 µmol/kg) is statistically indistinguishable from the modern ($p = 0.29$). Regardless, BWO concentrations in the LGM (84 ± 5 µmol/kg) were significantly lower ($p < 0.01$) than both the modern and the mean late Holocene (Fig. 8E).

The offset in U/Ba and $\Delta\delta^{13}C$ in the WEA is consistent with the positive bias in $\Delta\delta^{13}C$ observed in both the EEP and the Arabian Sea. In the EEP, $\Delta\delta^{13}C$-based BWO concentrations are 60–100 µmol/kg higher than those reconstructed by U/Ba, and in the Arabian Sea, $\Delta\delta^{13}C$-based BWO concentrations are greater by ~70 µmol/kg than those reconstructed by U/Ba and surface porosity. Shifting the WEA $\Delta\delta^{13}C$-based BWO concentrations down by similar offsets (60, 90, and 120 µmol/kg) better aligns the absolute values of U/Ba and $\Delta\delta^{13}C$ BWO concentrations (as noted in previous sections, the absolute values of mean U/Ba are more reliable than their relative trends). Interestingly, optimizing the agreement between U/Ba and $\Delta\delta^{13}C$ in the LGM requires a large offset (~120 µmol/kg), while no discrepancy is apparent in the Holocene. Temporally variable $\Delta\delta^{13}C$ offsets from U/Ba were also observed at site ODP1240 in the EEP, and this concurrence may imply that $\Delta\delta^{13}C$ is more sensitive than U/Ba to additional climate-related processes besides changes in BWO concentrations. At the Demerara Rise, the greater offset between U/Ba and $\Delta\delta^{13}C$ in the LGM relative to the Holocene corresponds with higher glacial organic carbon fluxes (e.g., Fig. 4B). More abundant organic matter would fuel respiration in the sediment and potentially intensify the anaerobic processes like denitrification that lower the $\delta^{13}C$ of *G. affinis*. As yet, the above exercise is only an empirical demonstration of the possibility, and future work is required to investigate whether or not this offset is a real signal and whether its magnitude may vary spatially or temporally.

## 6. Conclusions

U/Ba has potential to operate regionally as a quantitative proxy for BWO concentrations in the late Pleistocene (last 500,000 years). This new parameterization of uranium normalized to barium has advantages over previous parameterizations, such as authigenic uranium or uranium enrichment factors, by explicitly accounting for changes in organic carbon flux and minimizing the effects of variable sedimentation rates. Although there is no singular global relationship between U/Ba and BWO (Fig. 5A), more robust relationships emerge when the data are restricted to smaller spatial scales like ocean basins (Fig. 5B-E) and even smaller regional scales like the Eastern Equatorial Pacific (Fig. 6B), the Arabian Sea (Fig. 7B), and the Western Equatorial Atlantic (Fig. 8B). The test calibrations for each of these regions are distinct and non-transferrable, and they should not be applied to sites outside of the domain of the calibration. Future work in other areas will depend on the development of well-constrained, regionally specific core top calibrations.

In the three test regions, the U/Ba proxy performed well at capturing absolute BWO concentrations during mean climate states, like the Holocene and the Last Glacial Maximum. In the Eastern Equatorial Pacific, it was demonstrated that U/Ba is less well suited to capturing the timing of transient BWO variability due to potential remobilization effects from uranium burndown. U/Ba aligned better than $\Delta\delta^{13}C$ with 1) modern BWO concentrations and reconstructions from alkenone preservation (EEP) and 2) reconstructions from benthic foraminifera surface porosity (Arabian Sea). In all three regions the $\Delta\delta^{13}C$-based BWO concentrations appear to be skewed high on the order of 60–150 μmol/kg. This offset may indicate that denitrification by *Globobulimina spp*. and its effects on $\Delta\delta^{13}C$ are not taken into consideration as often as they perhaps should. Future proxy development of both U/Ba and $\Delta\delta^{13}C$, as well as other paleo-oxygen proxies, will continue to improve our ability to robustly reconstruct oxygen concentrations in the past.

## Declaration of Competing Interest

The authors declare that they have no known competing financial interests or personal relationships that could have appeared to influence the work reported in this paper.

## Acknowledgements

This work was improved by constructive feedback from Dr. Tom Jilbert and one anonymous reviewer. We thank the WHOI Seafloor Samples Repository for curating and providing the samples. K. Pietro provided analytical assistance. This work was funded by NSF grant OCE-1946185 (K.M.C., D.O.) and OCE-1829406 and OCE-1948716 (K.M.C. and S.G.N.). W. L. and Y. W. were supported by the WHOI Postdoctoral Scholar Program. All data are available in Supplementary Data 1 and 2.

## Appendix A. Supplementary material

Supplementary material includes one supplemental text on lithogenic corrections, two supplemental figures, and two data tables. These files can be found online at https://doi.org/10.1016/j.gca.2022.12.022.

## References

Altabet, M.A., Higginson, M.J., Murray, D.W., 2002. The effect of millennial-scale changes in Arabian Sea denitrification on atmospheric $CO_2$. Nature 415, 159–162.

Anderson, R.F., 1982. Concentration, vertical flux, and remineralization of particulate uranium in seawater. Geochim. Cosmochim. Acta 46, 1293–1299.

Anderson, R.F., Winckler, G., 2005. Problems with paleoproductivity proxies. Paleoceanography 20, 1–7.

Anderson, R.F., Fleisher, M.Q., LeHuray, A.P., 1989. Concentration, oxidation state, and particulate flux of uranium in the Black Sea. Geochim. Cosmochim. Acta 53, 2215–2224.

Anderson, R.F., Ali, S., Bradtmiller, L.I., Nielson, S.H.H., Fleisher, M.Q., Anderson, B.E., Burckle, L.H., 2009. Wind-driven upwelling in the Southern Ocean and the deglacial rise in atmospheric $CO_2$. Science 323, 1443–1448.

Anderson, R.F., Barker, S., Fleisher, M., Gersonde, R., Goldstein, S.L., Kuhn, G., Mortyn, P.G., Pahnke, K., Sachs, J.P., 2014. Biological response to millennial variability of dust and nutrient supply in the Subantarctic South Atlantic Ocean. Philos. Trans. R. Soc. London 372, 20130054.

Anderson, R.F., Sachs, J.P., Fleisher, M.Q., Allen, K.A., Yu, J., Koutavas, A., Jaccard, S.L., 2019. Deep-Sea oxygen depletion and ocean carbon sequestration during the last ice age. Global Biogeochem. Cycles 33.

Armstrong, R.A., Lee, C., Hedges, J.I., Honjo, S., Wakeham, S.G., 2001. A new, mechanistic model for organic carbon fluxes in the ocean based on the quantitative association of POC with ballast minerals. Deep Sea Res. Part II 49, 219–236.

Arndt, S., Jørgensen, B.B., LaRowe, D.E., Middelburg, J.J., Pancost, R.D., Regnier, P., 2013. Quantifying the degradation of organic matter in marine sediments: A review and synthesis. Earth Sci. Rev. 123, 53–86.

Barnes, C.E., Cochran, J.K., 1990. Uranium removal in oceanic sediments and the oceanic U balance. Earth Planet. Sci. Lett. 97, 94–101.

Baturin, G.N., Kochenov, A.V., 2001. Uranium in phosphorites. Lithol. Min. Resour. 36, 303–321.

Berger, W.H., Johnson, R.F., 1978. On the thickness and the 14C age of the mixed layer in deep-sea carbonates. Earth Planet. Sci. Lett. 41, 223–227.

Bertram, M.A., Cowen, J.P., 1997. Morphological and compositional evidence for biotic precipitation of marine barite. J. Mar. Res. 55, 577–593.

Bishop, J.K.B., 1988. The barite-opal-organic carbon association in oceanic particulate matter. Nature 332, 341–343.

Bonn, W.J., Gingele, F.X., Grobe, H., Mackensen, A., Fütterer, D.K., 1998. Palaeoproductivity at the Antarctic continental margin: opal and barium records for the last 400 ka. Palaeogeogr. Palaeoclimatol. Palaeoecol. 139, 195–211.

Boyle, E.A., 1990. Quaternary deepwater paleoceanography. Science 249, 863–870.

Bradtmiller, L.I., Anderson, R.F., Fleisher, M.Q., Burckle, L.H., 2007. Opal burial in the equatorial Atlantic Ocean over the last 30 ka: Implications for glacial-interglacial changes in the ocean silicon cycle. Paleoceanography 22.

Brüchert, V., Jørgensen, B.B., Neumann, K., Riechmann, D., Schlösser, M., Schulz, H., 2003. Regulation of bacterial sulfate reduction and hydrogen sulfide fluxes in the central Namibian coastal upwelling zone. Geochim. Cosmochim. Acta 67, 4505–4518.

Burdige, D.J., Gieskes, J.M., 1983. A pore water/solid phase diagenetic model for manganese in marine sediments. Am. J. Sci. 283, 29–47.

Cabré, A., Marinov, I., Bernardello, R., Bianchi, D., 2015. Oxygen minimum zones in the tropical Pacific across CMIP5 models: mean state differences and climate change trends. Biogeosciences 12, 5429–5454.

Calvert, S.E., Pedersen, T.F., 1993. Geochemistry of recent oxic and anoxic sediments: Implications for the geological record. Mar. Geol. 113, 67–88.

Calvert, S.E., Price, N.B., 1983. Geochemistry of Namibian shelf sediments. In: Suess, E. (Ed.), Coastal Upwelling and Its Sediment Record. Plenum Press, New York, NY, pp. 337–375.

Calvert, S.E., Piper, D.Z., Thunell, R.C., Astor, Y., 2015. Elemental settling and burial fluxes in the Cariaco Basin. Mar. Chem. 177, 607–629.

Calvo, E., Pelejero, C., Pena, L.D., Cacho, I., Logan, G.A., 2011. Eastern equatorial pacific productivity and related-$CO_2$ changes since the last glacial period. Proc. Natl. Acad. Sci. U. S. A. 108, 5537–5541.

Canfield, D.E., 1994. Factors influencing organic carbon preservation in marine sediments. Chem. geology 114 (3–4), 315–329.

Carter, S.C., Paytan, A., Griffith, E.M., 2020. Toward an improved understanding of the marine barium cycle and the application of marine barite as a paleoproductivity proxy. Minerals 10, 1–24.

Ceccaroni, L., Frank, M., Frignani, M., Langone, L., Ravaioli, M., Mangini, A., 1998. Late Quaternary fluctuations of biogenic component fluxes on the continental slope of the Ross Sea, Antarctica. J. Mar. Syst. 17, 515–525.

Chase, Z., Anderson, R.F., Fleisher, M.Q., Kubik, P.W., 2003. Scavenging of $^{230}Th$, $^{231}Pa$ and $^{10}Be$ in the Southern Ocean (SW Pacific sector): The importance of particle flux and advection. Deep Sea Res. Part II Top. Stud. Oceanogr. 50, 739–768.

Church, T.M., Wolgemuth, K., 1972. Marine barite saturation. Earth Planet. Sci. Lett. 15, 35–44.

Cochran, J.K., 1985. Particle mixing rates in sediments of the eastern equatorial Pacific: Evidence from $^{210}Pb$, $^{239,240}Pu$ and $^{137}Cs$ distributions at MANOP sites. Geochim. Cosmochim. Acta 49, 1195–1210.

Costa, K.M., McManus, J.F., 2017. Efficacy of $^{230}Th$ normalization in sediments from the Juan de Fuca Ridge, northeast Pacific Ocean. Geochim. Cosmochim. Acta 197, 215–225.

Costa, K.M., McManus, J.F., Anderson, R.F., Ren, H., Sigman, D.M., Winckler, G., Fleisher, M.Q., Marcantonio, F., Ravelo, A.C., 2016. No iron fertilization in the equatorial Pacific Ocean during the last ice age. Nature 529, 519–522.

Costa, K.M., Anderson, R.F., McManus, J.F., Winckler, G., Middleton, J.L., Langmuir, C. H., 2018. Trace element (Mn, Zn, Ni, V) and authigenic uranium (aU) geochemistry reveal sedimentary redox history on the Juan de Fuca Ridge, North Pacific Ocean. Geochim. Cosmochim. Acta 236, 79–98.

Costa, K.M., Hayes, C.M., Anderson, R.F., Pavia, F.J., Bausch, A., Deng, F., Dutay, J., Geibert, W., Heinze, C., Henderson, G., Hillaire-Marcel, C., Hoffmann, S., Jaccard, S.L., Jacobel, A.W., Kienast, S.S., Kipp, L., Lerner, P., Lippold, J., Lund, D., Marcantonio, F., McGee, D., McManus, J.F., Mekik, F., Middleton, J.L., Missiaen, L., Not, C., Pichat, S., Robinson, L.F., Rowland, G.H., Roy-Barman, M., Tagliabue, A., Torfstein, A., Winckler, G., Zhou, Y., 2020. 230Th normalization: New insights on an essential tool for quantifying sedimentary fluxes in the modern and Quaternary ocean. Paleoceanogr Paleoclimatol. 35.

Crusius, J., Calve, S., Pedersen, T., Sage, D., 1996. Rhenium and molybdenum enrichments in sediments as indicators of oxic, suboxic and sulfidic conditions of deposition. Earth Planet. Sci. Lett. 145, 65–78.

D'Errico, J., 2022. SLM - Shape Language Modeling. https://www.mathworks.com/matlabcentral/fileexchange/24443-slm-shape-language-modeling.

D'Hondt, S., Inagaki, F., Zarikian, C.A., Abrams, L.J., Dubois, N., Engelhardt, T., Evans, H., Ferdelman, T., Gribsholt, B., Harris, R.N., Hoppie, B.W., 2015. Presence of oxygen and aerobic communities from sea floor to basement in deep-sea sediments. Nat. Geosci. 8, 299–304.

Dehairs, F., Chesselet, R., Jedwab, J., 1980. Discrete suspended particles of barite and the barium cycle in the open ocean. Earth Planet. Sci. Lett. 49, 528–550.

D'Hondt, S., Spivack, A.J., Pockalny, R., Ferdelman, T.G., Fischer, J.P., Kallmeyer, J., Abrams, L.J., Smith, D.C., Graham, D., Hasiuk, F., Schrum, H., 2009. Subseafloor sedimentary life in the South Pacific Gyre. Proc. Natl. Acad. Sci. 106, 11651–11656.

Dorta, C.C., Rona, E., 1971. Geochemistry of Uranium in the Cariaco Trench. Bull. Mar. Sci., 754–765

Dymond, J., Suess, E., Lyle, M.W., 1992. Barium in deep-sea sediment: A geochemical proxy for paleoproductivity. Paleoceanography 7, 163–181.

Eagle, M., Paytan, A., Murray, R.W., 2003. A comparison between excess barium and barite as indicators of carbon export. Paleoceanography 18, 1–13.

Endrizzi, F., Rao, L., 2014. Chemical speciation of uranium(VI) in marine environments: Complexation of calcium and magnesium ions with [$(UO_2)(CO_3)3$]4-and the effect on the extraction of uranium from seawater. Chem. - A Eur. J. 20, 14499–14506.

Erdem, Z., Schönfeld, J., Rathburn, A.E., Pérez, M.E., Cardich, J., Glock, N., 2020. Bottom-water deoxygenation at the Peruvian margin during the last deglaciation recorded by benthic foraminifera. Biogeosciences 17, 3165–3182.

Fleisher, M.Q., Anderson, R.F., 2003. Assessing the collection efficiency of Ross Sea sediment traps using $^{230}$Th and $^{231}$Pa. Deep Sea Res. Part II Top. Stud. Oceanogr. 50, 693–712.

Francis, A.J., Dodge, C.J., Lu, F., Halada, G.P., Clayton, C.R., 1994. XPS and XANES studies of uranium reduction by Clostridium sp. Environ. Sci. Technol. 28, 636–639.

Francois, R., Honjo, S., Manganini, S.J., Ravizza, G.E., 1995. Biogenic barium fluxes to the deep sea: Implications for paleoproductivity reconstruction. Global Biogeochem. Cycles 9 (2), 289–303.

Frank, M., Eisenhauer, A., Bonn, W.J., Walter, P., Grobe, H., Kubik, P.W., Dittrich-Hannen, B., Mangini, A., 1995. Sediment redistribution versus paleoproductivity change: Weddell Sea margin sediment stratigraphy and biogenic particle flux of the barium profiles. Earth Planet. Sci. Lett. 136, 559–573.

Frank, M., Gersonde, R., Rutgers van der Loeff, M.M., Bohrmann, G., Nurnberg, C.C., Kubik, P.W., Suter, M., Mangini, A., 2000. Similar glacial and interglacial export bioproductivity in the Atlantic sector of the Southern Ocean : Multiproxy evidence and implications for glacial atmospheric $CO_2$. Paleoceanography 15, 642–658.

Froelich, P.N., Klinkhammer, G.P., Bender, M.L., Luedtke, N.A., Heath, G.R., Cullen, D., Dauphin, P., Hammond, D., Hartman, B., Maynard, V., 1979. Early oxidation of organic matter in pelagic sediments of the eastern equatorial Atlantic: suboxic diagenesis. Geochim. Cosmochim. Acta 43, 1075–1090.

Fu, W., Primeau, F., Moore, K.J., Lindsay, K., Randerson, J.T., 2018. Reversal of increasing tropical ocean hypoxia trends with sustained climate warming. Global Biogeochem. Cycles 32, 551–564.

Ganesh, R., Robinson, K.G., Reed, G.D., 1997. Reduction of hexavalent uranium from organic complexes by sulfate- and iron-reducing bacteria. Appl. Environ. Microbiol. 63, 4385–4391.

Ganeshram, R.S., François, R., Commeau, J., Brown-Leger, S.L., 2003. An experimental investigation of barite formation in seawater. Geochim. Cosmochim. Acta 67, 2599–2605.

Garcia, H.E., Cruzado, A., Gordon, L., Escanez, J., 1998. Decadal-scale chemical variability in the subtropical North Atlantic deduced from nutrient and oxygen data. J. Geophys. Res. 103, 2817–2830.

Garcia, H.E., Weathers, K., Paver, C.R., Smolyar, I., Boyer T.P., Locarnini, M.M., Zweng, M.M., Mishonov, A.V., Baranova, O.K., Seidov, D., Reagan, J.R., 2019. *World Ocean Atlas 2018, Volume 3: Dissolved Oxygen, Apparent Oxygen Utilization, and Dissolved Oxygen Saturation*. https://archimer.ifremer.fr/doc/00651/76337/.

Gaye, B., Böll, A., Segschneider, J., Burdanowitz, N., Emeis, K.-C., Ramaswamy, V., Lahajnar, N., Lückge, A., Rixen, T., 2018. Glacial–interglacial changes and Holocene variations in Arabian Sea denitrification. Biogeosciences 15, 507–527.

GEOTRACES Intermediate Data Product Group G., 2021. The GEOTRACES Intermediate Data Product 2021 (IDP2021).

Gonneea, M.E., Paytan, A., 2006. Phase associations of barium in marine sediments. Mar. Chem. 100, 124–135.

Gonzalez-Muñoz, M.T., Martinez-Ruiz, F., Morcillo, F., Martin-Ramos, J.D., Paytan, A., 2012. Precipitation of barite by marine bacteria: A possible mechanism for marine barite formation. Geology 40, 675–678.

Gouretski, V., Koltermann, K.P., 2004. *WOCE global hydrographic climatology*.

Hartnett, H.E., Keil, R.G., Hedges, J.I., Devol, A.H., 1998. Influence of oxygen exposure time on organic carbon preservation in continental margin sediments. Nature 391 (February), 572–575.

Hayes, C.T., Costa, K.M., Anderson, R.F., Calvo, E., Chase, Z., Demina, L.L., Dutay, J.C., German, C.R., Heimbürger-Boavida, L.E., Jaccard, S.L., Jacobel, A., Kohfeld, K.E., Kravchishina, M.D., Lippold, J., Mekik, F., Missiaen, L., Pavia, F.J., Paytan, A., Pedrosa-Pamies, R., Petrova, M.V., Rahman, S., Robinson, L.F., Roy-Barman, M., Sanchez-Vidal, A., Shiller, A., Tagliabue, A., Tessin, A.C., van Hulten, M., Zhang, J., 2021. Global ocean sediment composition and burial flux in the deep sea. Global Biogeochem. Cycles 35, 1–25.

Hickey, B., 2016. Reconstructing past flow rates of southern component water masses using sedimentary $^{231}$Pa/$^{230}$Th. University of Oxford. Ph.D dissertation.

Hoogakker, B.A.A., Elderfield, H., Schmiedl, G., McCave, I.N., Rickaby, R.E.M., 2015. Glacial-interglacial changes in bottom-water oxygen content on the Portuguese margin. Nat. Geosci. 8, 2–5.

Horner, T.J., Kinsley, C.W., Nielsen, S.G., 2015. Barium-isotopic fractionation in seawater mediated by barite cycling and oceanic circulation. Earth Planet. Sci. Lett. 430, 511–522.

Jaccard, S.L., Galbraith, E.D., Sigman, D.M., Haug, G.H., Francois, R., Pedersen, T.F., Dulski, P., Thierstein, H.R., 2009. Subarctic Pacific evidence for a glacial deepening of the oceanic respired carbon pool. Earth Planet. Sci. Lett. 277, 156–165.

Jaccard, S.L., Galbraith, E.D., 2012. Large climate-driven changes of oceanic oxygen concentrations during the last deglaciation. Nat. Geosci. 5, 151–156.

Jacobel, A.W., McManus, J.F., Anderson, R.F., Winckler, G., 2017. Repeated storage of respired carbon in the equatorial Pacific Ocean over the last three glacial cycles. Nat. Commun. 8.

Jacobel, A.W., Anderson, R.F., Jaccard, S.L., McManus, J.F., Pavia, F.J., Winckler, G., 2020. Deep Pacific storage of respired carbon during the last ice age: Perspectives from bottom water oxygen reconstructions. Quat. Sci. Rev. 230, 106065.

Jorissen, F.J., Fontanier, C., Thomas, E., 2007. Paleoceanographical proxies based on deep-sea benthic foraminiferal assemblage characteristics. Dev. Mar. Geol. 1, 263–325.

Kasten, Sabine, 2004. Porewater geochemistry of sediment core GeoB4418-3. PANGAEA, doi: 10.1594/PANGAEA.222556.

Keeling, R.F., Kortzinger, A., Gruber, N., 2010. Ocean deoxygenation in a warming world. Ann. Rev. Mar. Sci. 2, 199–229.

Keil, R.G., Montluçon, D.B., Prahl, F.G., Hedges, J.I., 1994. Sorptive preservation of labile organic matter in marine sediments. Nature 370, 549–552.

Klinkhammer, G.P., Palmer, M.R., 1991. Uranium in the oceans: Where it goes and why. Geochim. Cosmochim. Acta 55, 1799–1806.

Kochenov, A.V., Baturin, G.N., 2002. The paragenesis of organic matter, phosphorus, and uranium in marine sediments. Lithol. Miner. Resour. 37, 107–120.

Kochenov, A.V., Korloev, K.G., Dubinchuk, V.T., Medvedev, Y.L., 1977. Experimental data on the conditions of precipitation of uranium from aqueous solutions. Geochemistry Int. 14, 82–87.

Küster-Heins, K., Steinmetz, E., De Lange, G.J., Zabel, M., 2010. Phosphorus cycling in marine sediments from the continental margin off Namibia. Mar. Geol. 274, 95–106.

Kuwabara, J.S., Geen, A.V., McCorkle, D.C., Bernhard, J.M., 1999. Dissolved sulfide distributions in the water column and sediment pore waters of the Santa Barbara Basin. Geochim. Cosmochim. Acta 63, 2199–2209.

Langmuir, D., 1978. Uranium solution-mineral equilibria at low temperatures with applications to sedimentary ore deposits. Geochim. Cosmochim. Acta 42, 547–569.

Lee, S.Y., Cha, W.S., Kim, J.G., Baik, M.H., Jung, E.C., Jeong, J.T., Kim, K., Chung, S.Y., Lee, Y.J., 2014. Uranium (IV) remobilization under sulfate reducing conditions. Chem. Geol. 370, 40–48.

Lee, C., Wakeham, S., Arnosti, C., 2004. Particulate organic matter in the sea: the composition conundrum. AMBIO: A J. Human Environ. 33, 565–575.

Lee, T.R., Wood, W.T., Phrampus, B.J., 2019. A machine learning (kNN) approach to predicting global seafloor total organic carbon. Global Biogeochem. Cycles 33, 37–46.

Liger, E., Charlet, L., Van Cappellen, P., 1999. Surface catalysis of uranium (VI) reduction by iron (II). Geochim. Cosmochim. Acta 63, 2939–2955.

Lippold, J., Gutjahr, M., Blaser, P., Christner, E., de Carvalho Ferreira, M.L., Mulitza, S., Christl, M., Wombacher, F., Böhm, E., Antz, B., Cartapanis, O., Vogel, H., Jaccard, S.L., 2016. Deep water provenance and dynamics of the (de)glacial Atlantic meridional overturning circulation. Earth Planet. Sci. Lett. 445, 68–78.

Loveley, M.R., Marcantonio, F., Wisler, M.M., Hertzberg, J.E., Schmidt, M.W., Lyle, M. W., 2017. Millennial-scale iron fertilization of the eastern equatorial Pacific over the past 100,000 years. Nat. Geosci. 10, 1–4.

Lovley, D.R., Phillips, E.J., 1992. Reduction of uranium by Desulfovibrio desulfuricans. Appl. Environ. Microbiol. 58, 850–856.

Lovley, D.R., Phillips, E.J.P., Gorby, Y.A., Landa, E.R., 1991. Microbial reduction of Uranium. Nature 350, 413–416.

Lu, W., Rickaby, R.E.M., Hoogakker, B.A.A., Rathburn, A.E., Burkett, A.M., Dickson, A.J., Martínez-Méndez, G., Hillenbrand, C.D., Zhou, X., Thomas, E., Lu, Z., 2020. I/Ca in epifaunal benthic foraminifera: A semi-quantitative proxy for bottom water oxygen in a multi-proxy compilation for glacial ocean deoxygenation. Earth Planet. Sci. Lett. 533, 116055.

Lu, W., Barbosa, C.F., Rathburn, A.E., Xavier, P. da M., Cruz, A.P.S., Thomas, E., Rickaby, R.E.M., Zhang, Y.G., Lu, Z., 2021. Proxies for paleo-oxygenation: A downcore comparison between benthic foraminiferal surface porosity and I/Ca. Palaeogeogr. Palaeoclimatol. Palaeoecol. 579, 110588.

Lu, W., Wang, Y., Oppo, D.W., Nielsen, S.G., Costa, K.M., 2022. Comparing paleo-oxygenation proxies (benthic foraminiferal surface porosity, I/Ca, authigenic uranium) on modern sediments and the glacial Arabian Sea. Geochim. Cosmochim. Acta 331, 69–85.
Mangini, A., Jung, M., Laukenmann, S., 2001. What do we learn from peaks of uranium and of manganese in deep sea sediments? Mar. Geol. 177, 63–78.
Martínez-Garcia, A., Rosell-Melé, A., Geibert, W., Gersonde, R., Masqué, P., Gaspari, V., Barbante, C., 2009. Links between iron supply, marine productivity, sea surface temperature, and $CO_2$ over the last 1.1 Ma. Paleoceanography 24.
Martinez-Ruiz, F., Jroundi, F., Paytan, A., Guerra-Tschuschke, I., Abad, M.D.M., González-Muñoz, M.T., 2018. Barium bioaccumulation by bacterial biofilms and implications for Ba cycling and use of Ba proxies. Nat. Commun. 9, 1–9.
Martinez-Ruiz, F., Paytan, A., Gonzalez-Muñoz, M.T., Jroundi, F., Abad, M.M., Lam, P. J., Bishop, J.K.B., Horner, T.J., Morton, P.L., Kastner, M., 2019. Barite formation in the ocean: Origin of amorphous and crystalline precipitates. Chem. Geol. 511, 441–451.
Matear, R.J., Hirst, A.C., 2003. Long-term changes in dissolved oxygen concentrations in the ocean caused by protracted global warming. Global Biogeochem. Cycles 17, 1125.
McCorkle, D.C., Emerson, S.R., 1988. The relationship between pore water carbon isotopic composition and bottom water oxygen concentration. Geochim. Cosmochim. Acta 52, 1169–1178.
McManus, J., Berelson, W.M., Klinkhammer, G.P., Johnson, K.S., Coale, K.H., Anderson, R.F., Kumar, N., Burdige, D.J., Hammond, D.E., Brumsack, H.J., McCorkle, D.C., Rushdi, A., 1998. Geochemistry of barium in marine sediments: implications for its use as a paleoproxy. Geochim. Cosmochim. Acta 62, 3453–3473.
McManus, J., Berelson, W.M., Klinkhammer, G.P., Hammond, D.E., Holm, C., 2005. Authigenic uranium: relationship to oxygen penetration depth and organic carbon rain. Geochim. Cosmochim. Acta 69, 95–108.
McManus, J., Berelson, W.M., Severmann, S., Poulson, R.L., Hammond, D.E., Klinkhammer, G.P., Holm, C., 2006. Molybdenum and uranium geochemistry in continental margin sediments: Paleoproxy potential. Geochim. Cosmochim. Acta 70, 4643–4662.
Middelburg, J.J., 1991. Organic carbon, sulphur, and iron in recent semi-euxinic sediments of Kau Bay, Indonesia. Geochim. Cosmochim. Acta 55, 815–828.
Mills, R.A., Taylor, S.L., Pälike, H., Thomson, J., 2010. Hydrothermal sediments record changes in deep water oxygen content in the SE Pacific. Paleoceanography 25, PA4226.
Monnin, C., Jeandel, C., Cattaldo, T., Dehairs, F., 1999. The marine barite saturation state of the world's oceans. Mar. Chem. 65, 253–261.
Morford, J.L., Emerson, S., 1999. The geochemistry of redox sensitive trace metals in sediments. Geochim. Cosmochim. Acta 63, 1735–1750.
Morford, J.L., Martin, W.R., Carney, C.M., 2009. Uranium diagenesis in sediments underlying bottom waters with high oxygen content. Geochim. Cosmochim. Acta 73, 2920–2937.
Müller, P.J., Suess, E., 1979. Productivity, sedimentation rate, and sedimentary organic matter in the oceans-I. Organic carbon preservation. Deep Sea Res. Part A 26 (12), 1347–1362.
Murray, R.W., Knowlton, C., Leinen, M., Mix, A.C., Polsky, C.H., 2000. Export production and carbonate dissolution in the central equatorial Pacific Ocean over the past 1 Myr. Paleoceanography 15, 570–592.
Nakashima, S., Disnar, J.-R., Perruchot, A., Trichet, J., 1984. Experimental study of mechanisms of fixation and reduction of uranium by sedimentary organic matter under diagenetic or hydrothermal conditions. Geochim. Cosmochim. Acta 48, 2321–2329.
Nameroff, T.J., Balistrieri, L.S., Murray, J.W., 2002. Suboxic trace metal geochemistry in the eastern tropical North Pacific. Geochim. Cosmochim. Acta 66, 1139–1158.
Neimann, S., Geibert, W., 2003. $^{231}$Pa ex and $^{230}$Th ex at the southeast South American continental margin - Is the $^{231}$Pa ex / $^{230}$Th ex ratio a proxy for particle flux or ocean circulation? Freie Universi√§t, Berlin. Ph.D. dissertation.
Nomaki, H., Chikaraishi, Y., Tsuchiya, M., Toyofuku, T., Suga, H., Sasaki, Y., Uematsu, K., Tame, A., Ohkouchi, N., 2015. Variation in the nitrogen isotopic composition of amino acids in benthic foraminifera: Implications for their adaptation to oxygen-depleted environments. Limnol. Oceanogr. 60, 1906–1916.
Ohkushi, K., Kennett, J.P., Zeleski, C.M., Moffitt, S.E., Hill, T.M., Robert, C., Beaufort, L., Behl, R.J., 2013. Quantified intermediate water oxygenation history of the NE Pacific: A new benthic foraminiferal record from Santa Barbara basin. Paleoceanography 28, 453–467.
Olsen, A., Key, R.M., Van Heuven, S., Lauvset, S.K., Velo, A., Lin, X., Schirnick, C., Kozyr, A., Tanhua, T., Hoppema, M., Jutterström, S., Steinfeldt, R., Jeansson, E., Ishii, M., Pérez, F.F., Suzuki, T., 2016. The global ocean data analysis project version 2 (GLODAPv2) - An internally consistent data product for the world ocean. Earth Syst. Sci. Data 8, 297–323.
Oppo, D.W., Gebbie, G., Huang, K., 2018. Data constraints on glacial atlantic water mass geometry and properties. Paleoceanogr. Paleoclimatol. 33, 1013–1034.
Orsi, A.H., Whitworth, T., Nowlin, W.D., 1995. On the meridional extent and fronts of the Antarctic Circumpolar Current. Deep-Sea Res. I 42, 641–673.
Oschlies, A., Schulz, K.G., Riebesell, U., Schmittner, A., 2008. Simulated 21st century's increase in oceanic suboxia by $CO_2$-enhanced biotic carbon export. Global Biogeochem. Cycles 22, GB4008.
Owens, S.A., Buesseler, K.O., Sims, K.W.W., 2011. Re-evaluating the $^{238}$U-salinity relationship in seawater: Implications for the $^{238}$U–$^{234}$Th disequilibrium method. Mar. Chem. 127, 31–39.
Palter, J.B., Trossman, D.S., 2018. The sensitivity of future ocean oxygen to changes in ocean circulation. Global Biogeochem. Cycles 32, 738–751.
Paytan, A., Kastner, M., 1996. Benthic Ba fluxes in the central Equatorial Pacific, implications for the oceanic Ba cycle. Earth Planet. Sci. Lett. 142, 439–450.
Paytan, A., Kastner, M., Chavez, F.P., 1996. Glacial to interglacial fluctuations in productivity in the equatorial Pacific as indicated by marine barite. Science 274 (5291), 1355–1357.
Pfeifer, K., Kasten, S., Hensen, C., Schulz, H.D., 2001. Reconstruction of primary productivity from the barium contents in surface sediments of the South Atlantic Ocean. Mar. Geol. 177, 13–24.
Pilson, M.E., 2012. An Introduction to the Chemistry of the Sea. Cambridge University Press.
Piña-Ochoa, E., Koho, K., Geslin, E., Risgaard-Petersen, N., 2010. Survival and life strategy of the foraminiferan Globobulimina turgida through nitrate storage and denitrification. Mar. Ecol. Prog. Ser. 417, 39–49.
Prahl, F.G., Collier, R.B., Dymond, J., Lyle, M., Sparrow, M.A., 1993. A biomarker perspective on prymnesiophyte productivity in the northeast pacific ocean. Deep. Res. Part I 40, 2061–2076.
Prakash Babu, C., Brumsack, H.J., Schnetger, B., Böttcher, M.E., 2002. Barium as a productivity proxy in continental margin sediments: A study from the eastern Arabian Sea. Mar. Geol. 184, 189–206.
Rathburn, A.E., Willingham, J., Ziebis, W., Burkett, A.M., Corliss, B.H., 2018. A New biological proxy for deep-sea paleo-oxygen: Pores of epifaunal benthic foraminifera. Sci. Rep. 8, 1–8.
Raven, M.R., Sessions, A.L., Fischer, W.W., Adkins, J.F., 2016. Sedimentary pyrite δ34S differs from porewater sulfide in Santa Barbara Basin: Proposed role of organic sulfur. Geochim. Cosmo. Acta 186, 120–134.
Reichart, G.J., Schenau, S.J., De Lange, G.J., Zachariasse, W.J., 2002. Synchroneity of oxygen minimum zone intensity on the Oman and Pakistan Margins at sub-Milankovitch time scales. Mar. Geol. 185, 403–415.
Reimers, C.E., Lange, C., Tabak, M., Bernhard, J.M., 1990. Seasonal spillover and varve formation in the Santa Barbara Basin, California. Limn. Ocean 35, 1577–1585.
Reimers, C.E., Ruttenberg, K.C., Canfield, D.E., Christiansen, M.B., Martin, J.B., 1996. Porewater pH and authigenic phases formed in the uppermost sediments of Santa Barbara Basin. Geochim. Cosmochim. Acta 60, 4037–4057.
Rodrigo-Gámiz, M., Rampen, S.W., Schouten, S., Sinninghe Damsté, J.S., 2016. The impact of oxic degradation on long chain alkyl diol distributions in Arabian Sea surface sediments. Org. Geochem. 100, 1–9.
Russell, A.D., Hönisch, B., Spero, H.J., Lea, D.W., 2004. Effects of seawater carbonate ion concentration and temperature on shell U, Mg, and Sr in cultured planktonic foraminifera. Geochim. Cosmochim. Acta 68, 4347–4361.
Sani, R.K., Peyton, B.M., Amonette, J.E., Geesey, G.G., 2004. Reduction of uranium (VI) under sulfate-reducing conditions in the presence of Fe (III)-(hydr)oxides. Geochim. Cosmochim. Acta 68, 2639–2648.
Sarin, M.M., Borole, D.V., Krishnaswami, S., 1979. Geochemistry and geochronology of sediments from the Bay of Bengal and the equatorial Indian Ocean. Proc. Indian Acad. Sci. - Earth Planet. Sci. 88A, 131–154.
Sarkar, A., Bhattacharya, S.K., Sarin, M.M., 1993. Geochemical evidence for anoxic deep water in the Arabian Sea during the last glaciation. Geochim. Cosmochim. Acta 57, 1009–1016.
Schenau, S.J., Prins, M.A., De Lange, Monnin, C., 2001. Barium accumulation in the Arabian Sea: Controls on barite preservation in marine sediments. Geochim. Cosmochim. Acta 65 (10), 1545–1556.
Schoepfer, S.D., Shen, J., Wei, H., Tyson, R.V., Ingall, E., Algeo, T.J., 2015. Total organic carbon, organic phosphorus, and biogenic barium fluxes as proxies for paleomarine productivity. Earth-Science Rev. 149, 23–52.
Serno, S., Winckler, G., Anderson, R.F., Hayes, C.T., McGee, D., Machalett, B., Ren, H., Straub, S.M., Gersonde, R., Haug, G.H., 2014. Eolian dust input to the Subarctic North Pacific. Earth Planet. Sci. Lett. 387, 252–263.
Sharon, Belanger, C.L., 2022. Placing North Pacific paleo-oxygenation records on a common scale using multivariate analysis of benthic foraminiferal assemblages. Quat. Sci. Rev. 280.
Shigemitsu, M., Narita, H., Watanabe, Y.W., Harada, N., Tsunogai, S., 2007. Ba, Si, U, Al, Sc, La, Th, C and $^{13}$C/$^{12}$C in a sediment core in the western subarctic Pacific as proxies of past biological production. Mar. Chem. 106, 442–455.
Shipboard Scientific Party, 1989. Site 727. In Prell, W.L., Niitsuma, N., et al., Proc. ODP, Init. Repts., 117: College Station, TX (Ocean Drilling Program), 467–493. doi:10.2973/odp.proc.ir.117.114.1989.
Shipboard Scientific Party, 2003. Site 1240. In Mix, A.C., Tiedemann, R., Blum, P., et al., Proc. ODP, Init. Repts., 202: College Station, TX (Ocean Drilling Program), 1–82. doi:10.2973/odp.proc.ir.202.111.2003.
Sigman, D.M., Boyle, E.A., 2000. Glacial/interglacial variationsin atmospheric carbon dioxide. Nature 407, 859–869.
Sigman, D.M., Hain, M.P., Haug, G.H., 2010. The polar ocean and glacial cycles in atmospheric $CO_2$ concentration. Nature 466, 47–55.
Singh, A.K., Marcantonio, F., Lyle, M.W., 2011. Sediment focusing in the panama basin, eastern equatorial pacific ocean. Earth Planet. Sci. Lett. 309, 33–44.
Singh, A.K., Marcantonio, F., Lyle, M., 2020. An assessment of xsBa flux as a paleoproductivity indicator and its water-depth dependence in the easternmost equatorial pacific ocean. Paleoceanogr. Paleoclimatol. 35, 1–17.
Sirocko, F., Garbe-Schonberg, D., Devey, C., 2000. Processes controlling trace element geochemistry of Arabian Sea sediments during the last 25,000 years. Glob. Planet. Change 26, 217–303.
Stramma, L., Johnson, G.C., Sprintall, J., Mohrholz, V., 2008. Expanding oxygen-minimum zones in the tropical oceans. Science 320, 655–659.
Stramma, L., Oschlies, A., Schmidtko, S., 2012. Mismatch between observed and modeled trends in dissolved upper-ocean oxygen over the last 50 yr. Biogeosciences 9, 4045–4057.

Taylor, S.R., McLennan, S.M., 1995. The geochemical evolution of the continental crust. Rev. Geophys. 33, 241–265.
Tetard, M., Licari, L., Beaufort, L., 2017. Oxygen history off Baja California over the last 80 kyr: A new foraminiferal-based record. Paleoceanography, 246–264.
Tetard, M., Ovsepyan, E., Licari, L., 2021. Eubuliminella tenuata as a new proxy for quantifying past bottom water oxygenation. Mar. Micropaleontol. 166, 102016.
Thorton, S.E., 1984. Basin model for hemipelagic sedimentation in a tectonically active continental margin: Santa Barbara Basin, California Continental Borderland. In: Geological Society, London, Special Publications, London, United Kingdom. Vol.15, pp. 377–394.
Torres, M.E., Brumsack, H.J., Bohrmann, G., Emeis, K.-C., 1996. Barite fronts in continental margin sediments: a new look at barium remobilization in the zone of sulfate reduction and formation of heavy barites in diagenetic fronts. Chem. Geol. 127, 125–139.
Trauth, M.H., 2013. TURBO2: A MATLAB simulation to study the effects of bioturbation on paleoceanographic time series. Comput. Geosci. 61, 1–10.
Veeh, H.H., Heggie, D.T., Crispe, A.J., 1999. Biogeochemistry of southern Australian continental slope sediments. Aust. J. Earth Sci. 46, 563–575.
Veeh, H.H., McCorkle, D.C., Heggie, D., 2000. Glacial/interglacial variations of sedimentation on the West Australian continental margin: constraints from excess $^{230}$Th. Mar. Geol. 166, 11–30.
Von Breymann, M.T., Brumsack, H.J., Emeis, K.-C., Camerlenghi, A., 1992. Depositional and Diagenetic Behavior of Barium in the Japan Sea. In: Proceedings of the Ocean Drilling Program, 127/128 Scientific Results College Station, TX, USA. pp. 651–665.
Wang, Y., Lu, W., Costa, K.M., Nielsen, S.G., 2022. Beyond anoxia: exploring sedimentary thallium isotopes in paleo-redox reconstructions from a new core top collection. Geochim. Cosmochim. Acta 333, 347–361.
Weber, M.E., 1998. Estimation of biogenic carbonate and opal by continuous non-destructive measurements in deep-sea sediments: application to the eastern Equatorial Pacific. Deep Sea Res. Part I Oceanogr. Res. Pap. 45, 1955–1975.
Zheng, Y., Anderson, R.F., Geen, A.V., Fleisher, M.Q., 2002. Preservation of particulate non-lithogenic uranium in marine sediments. Geochim. Cosmochim. Acta 66, 3085–3092.